

Non-ergodic inference for stationary-increment harmonizable stable processes

Ly Viet Hoang, Evgeny Spodarev

Ulm University

Abstract

We consider the class of stationary-increment harmonizable stable processes with infinite control measure, which most notably includes real harmonizable fractional stable motions. We give conditions for the integrability of the paths of such processes with respect to a finite, absolutely continuous measure and derive the distributional characteristics of the path integral with respect to said measure. The convolution of the path of a stationary-increment harmonizable stable process with a suitable measure yields a real stationary harmonizable stable process with finite control measure. This allows us to construct consistent estimators for the index of stability as well as the kernel function in the integral representation of a stationary increment harmonizable stable process (up to a constant factor). For real harmonizable fractional stable motions consistent estimators for the index of stability and its Hurst parameter are given. These are computed directly from the periodogram frequency estimates of the smoothed process.

Keywords:

Fourier analysis, fractional stable motion, frequency estimation, Hurst parameter, harmonizable process, non-ergodic process, non-ergodic statistics, periodogram, spectral density estimation, stable process, process with stationary increments

1. Introduction

A stochastic process or random field $X = \{X(t) : t \in T\}$ is called *self-similar* with index H or H -self-similar if it is invariant in distribution under scaling of time and space. Specifically, the processes $\{X(at) : t \in T\}$ and $\{a^H X(t) : t \in T\}$ are equal in distribution, meaning that all their finite dimensional distributions are equal. Furthermore, X has *stationary increments* if for all $h \in T$ the processes $\{X(t+h) - X(h) : t \in T\}$ and $\{X(t) - X(0) : t \in T\}$ have identical finite-dimensional distributions. A classical example of a self-similar stochastic process with stationary increments is the fractional Brownian motion, a process widely used for modeling phenomena in finance, telecommunications or natural sciences such as hydrology since self-similar objects (or fractals) are abundant in nature [23, 24, 26, 29, 30, 31, 32].

Fractional Brownian motions are characterized by their *Hurst parameter* or *exponent* $H \in (0, 1)$ and generalize the classical Brownian motion or Wiener process ($H = 0.5$). In fact, the

Email addresses: ly.hoang@uni-ulm.de (Ly Viet Hoang), evgeny.spodarev@uni-ulm.de (Evgeny Spodarev)

Preprint submitted to Elsevier

August 20, 2024

roughness of a fractional Brownian motion's path, its memory as well as the dependency between its increments are determined by the Hurst parameter. Moreover, fractional Brownian motions are self-similar with index H [16]. Furthermore, practical problems such as modeling of networks show that besides self-similarity heavy tailed distributions are of crucial importance as well [34, 42]. Hence, the extension to stable distributions is natural.

A fractional Brownian motion admits both a moving average as well as a harmonizable representation [40, Chapter 7.2]. The generalization of its moving average representation to the α -stable regime with $0 < \alpha < 2$ yields the class of linear fractional stable motions (LFSMs), whereas the extension of the harmonizable representation results in the class of harmonizable fractional stable motions (HFSMs) [11, 39], see also [25] and [40, Chapter 7.4, 7.7] for an overview. It is important to emphasize that the class of LFSMs and the class of HFSMs are disjoint for $0 < \alpha < 2$. Most notably, HFSMs are non-ergodic [13], hence statistical inference based on empirical averages is not possible.

Statistical inference of fractional Brownian motions has been studied extensively in [14, 17, 28], see [9] for an overview. A selection of works on the statistical inference for LFSMs is given by [3, 4, 8, 27, 33, 41], whereas HFSMs have not received as much attention in this regard due to their non-ergodicity. Only in recent years a handful of theoretical results on HFSMs have been published. Most notably, [7] presents the asymptotic theory for quadratic variations of HFSMs, [2, 6, 5] show path properties and a series representation for HFSMs, whereas [10] considers the more general class of operator scaling harmonizable random fields.

None of the above works on HFSMs consider point estimation of the stability index and Hurst parameter. Solely the preprint [1] proposes a framework for the simultaneous estimation of the index of stability and Hurst parameter based on wavelet transformations of the path of a HFSM, from which independent symmetric α -stable random variables are obtained. Their scale parameters are closely related to the index of stability and Hurst parameter. Although appealing in theory, this method relies on knowledge of the whole path of a HFSM on the real line since the required wavelets are oscillating functions at their tails, which is unfeasible from a practical point of view.

Throughout this paper we consider $\alpha \in (0, 2)$. We consider the broader class of stationary-increment harmonizable processes $X = \{X(t) : t \in \mathbb{R}\}$ with integral representation

$$X(t) = \operatorname{Re} \left(\int_{\mathbb{R}} (e^{itx} - 1) \Psi(x) M_{\alpha}(dx) \right), \quad t \in \mathbb{R},$$

where M_{α} is a complex isotropic symmetric α -stable random measure with Lebesgue control measure. The spectral density $\Psi \in L^{\alpha}(\mathbb{R}, \min(1, |x|^{\alpha})dx)$ characterizes the process uniquely. For the special choice $\Psi(x) = |x|^{-H-1/\alpha}$ the process X is a real HFSM. In this paper, we give consistent estimators for the index of stability α and the kernel function Ψ (up to a constant factor). In case of real HFSMs, consistent estimators for α as well as the Hurst parameter H are obtained. Our method is motivated by [1] but relies only on suitable convolutions of a single path of X making it effectively a smoothing procedure. There are only minimal constraints on the smoothing kernel (the so-called mollifier). Thus, choosing a mollifier with exponentially decaying tails is possible, ensuring that our method is highly practical.

The paper is structured as follows. In Section 2, we give basic notation and definitions on α -stable laws. Furthermore, complex $S\alpha S$ random measures and processes are introduced. The class of stationary real harmonizable stable processes with finite control measure and its properties are discussed, and the challenges of statistical inference on these processes are highlighted.

We also briefly introduce the periodogram frequency and spectral density estimation for stationary real harmonizable stable processes from [21]. The section concludes with posing the problem of estimating the index of stability α and spectral density Ψ for harmonizable stable processes with infinite control measure, in particular for real harmonizable fractional stable motions.

We consider the mollified or smoothed version of a stationary-increment harmonizable stable process in Section 3. Conditions on the smoothing kernel for a well-defined smoothing procedure are given. In fact, the smoothing kernel can be chosen such that the resulting smoothed process is stationary real harmonizable $S\alpha S$ process with finite control measure.

Section 4 focuses on the statistical inference on stationary-increment harmonizable stable processes as well as real harmonizable fractional stable motions. We first consider the more general class of stationary-increment harmonizable stable processes in Section 4.2. We give a strongly consistent estimator for the index of stability α based on two differently smoothed versions of the same path. Kernel density estimation on the frequencies in each mollified process, respectively, as well as linear regression on the logarithm of the ratio of the two kernel density estimators lead to the assessment of α . Furthermore, a consistent estimator for the spectral density Ψ up to a constant factor is given.

The special case of real harmonizable fractional stable motions is then considered in Section 4.3. We give a class of exponentially decaying smoothing kernels yielding a mollified process which is again stationary real harmonizable $S\alpha S$. The absolute p -th power (where $p \geq 1$ coincides with the rate of decay of the smoothing kernel at the origin) of the underlying random frequencies in the LePage series representation can be shown to be i.i.d. Gamma distributed. This allows us to compute the index of stability α and the Hurst parameter H directly from a combination of periodogram frequency estimation and consistent inference on the parameters of a Gamma distribution.

Lastly, we give an extensive numerical analysis in a simulation study in Section 5 and conclude our work with the discussion in Section 6.

2. Preliminaries

The following notation is used throughout this work. For any complex number $z \in \mathbb{C}$ we denote its real and imaginary part by $Re(z) = z^{(1)}$ and $Im(z) = z^{(2)}$, respectively. The notation $|\cdot|$ is both used for the absolute value on \mathbb{R} as well as on \mathbb{C} , where $|z| = \left((z^{(1)})^2 + (z^{(2)})^2\right)^{1/2}$ for $z \in \mathbb{C}$.

Let (E, \mathcal{E}, μ) be a measurable space. We define the space $L^p(E, \mu)$ with $0 < p < \infty$, i.e. the space p -integrable functions with respect to a measure μ on some measurable space E , by

$$L^p(E, \mu) = \left\{ u : E \rightarrow \mathbb{C} : \int_E |u(x)|^p \mu(dx) < \infty \right\}.$$

We write $\|u\|_{L^p(E, \mu)} = \left(\int_E |u(x)|^p \mu(dx)\right)^{1/p}$. Furthermore, we denote the space of p -integrable functions on \mathbb{R} with respect to the Lebesgue measure on \mathbb{R} simply by $L^p(\mathbb{R})$ and write $\|u\|_p = \left(\int_{\mathbb{R}} |u(x)|^p dx\right)^{1/p}$. The notation $\|\cdot\|_{\infty}$ stands for the uniform norm.

Denote by $\mathcal{L}^0(\Omega)$ the space of real-valued random variables on the probability space (Ω, \mathcal{F}, P) . Additionally, let $\mathcal{L}_c^0(\Omega) = \{X = X^{(1)} + iX^{(2)} : X^{(1)}, X^{(2)} \in \mathcal{L}^0(\Omega)\}$ be the space of complex-valued random variables. We write $X \stackrel{d}{=} Y$ if the random elements X and Y are equal in distribution.

In particular, for random processes (or fields) this means equality of their finite dimensional distributions.

A random variable $X \in \mathcal{L}^0(\Omega)$ is *symmetric α -stable ($S\alpha S$)* with *index of stability* $\alpha \in (0, 2]$ and *scale parameter* $\sigma > 0$, i.e. $X \sim S\alpha S(\sigma)$, if its characteristic function is given by

$$\mathbb{E} \left[e^{isX} \right] = \exp \{ -\sigma^\alpha |s|^\alpha \}.$$

Note that in the case $\alpha = 2$ the random variable X is Gaussian with mean 0 and variance $2\sigma^2$. Additionally, a \mathbb{R}^n -valued random vector $\mathbf{X} = (X_1, \dots, X_n)$ is $S\alpha S$ if its joint-characteristic function is of the form

$$\mathbb{E} [\exp \{i(\mathbf{s}, \mathbf{X})\}] = \exp \left\{ - \int_{S^{n-1}} |(\boldsymbol{\theta}, \mathbf{s})|^\alpha \Gamma(d\boldsymbol{\theta}) \right\},$$

where S^{n-1} is the Euclidean unit sphere in \mathbb{R}^n and (\cdot, \cdot) denotes the scalar product of two vectors in \mathbb{R}^n . The measure Γ on S^{n-1} is the *spectral measure* of \mathbf{X} . This measure is unique, finite and symmetric for $0 < \alpha < 2$ [40, Theorem 2.4.3]. A random variable $X \in \mathcal{L}_c^0(\Omega)$ is said to be $S\alpha S$ if $(X^{(1)}, X^{(2)}) = (Re(X), Im(X))$ is a $S\alpha S$ random vector.

Consider the measurable spaces (E, \mathcal{E}) and $(S^1, \mathcal{B}(S^1))$, where $\mathcal{B}(S^1)$ is the Borel- σ -algebra on the unit circle S^1 . For a measure k on the product space $(E \times S^1, \mathcal{E} \times \mathcal{B}(S^1))$, define the space $\mathcal{E}_0 = \{A \in \mathcal{E} : k(A \times S^1) < \infty\}$. A *complex $S\alpha S$ random measure* on (E, \mathcal{E}) is σ -additive, complex-valued set function $M_\alpha : \mathcal{E}_0 \rightarrow \mathcal{L}_c^0(\Omega)$, mapping into the space of complex random variables, such that M_α is independently scattered, i.e. $M_\alpha(A)$ and $M_\alpha(B)$ are independent for $A, B \in \mathcal{E}_0$ disjoint, and $M_\alpha(A)$ is a complex $S\alpha S$ random variable for all $A \in \mathcal{E}_0$. The $S\alpha S$ random vector $(M_\alpha^{(1)}(A), M_\alpha^{(2)}(A))$ has spectral measure $\Gamma_A = k(A \times \cdot)$ on $(S^1, \mathcal{B}(S^1))$. The measure k is called *circular control measure*, whereas the measure $m = k(\cdot \times S^1)$ on (E, \mathcal{E}_0) is referred to as *control measure* of M_α [40, Definition 6.1.2].

It holds that integration with respect to a $S\alpha S$ random measure M_α of the form $I(u) = \int_E u(x) M_\alpha(dx)$ is well-defined for $u \in L^\alpha(E, m)$ [40, Chapter 6.2]. Setting $(E, \mathcal{E}) = (\mathbb{R}, \mathcal{B}(\mathbb{R}))$, where $\mathcal{B}(\mathbb{R})$ is the Borel σ -algebra on \mathbb{R} , allows us to define complex-valued $S\alpha S$ random processes. For any $t \in \mathbb{R}$ let $h_t(\cdot)$ be a complex-valued function in $L^\alpha(\mathbb{R}, m)$. Then, the complex-valued $S\alpha S$ process $X = \{X(t) : t \in \mathbb{R}\}$ is defined by its integral representation

$$X(t) = \int_{\mathbb{R}} h_t(x) M_\alpha(dx), \quad t \in \mathbb{R}, \quad (1)$$

where M_α is a complex $S\alpha S$ random measure.

In particular, the case of complex *isotropic $S\alpha S$* measures is of interest. The random measure M_α is isotropic if $e^{i\phi} M_\alpha(A) \stackrel{d}{=} M_\alpha(A)$ holds for any $\phi \in [0, 2\pi)$ and $A \in \mathcal{E}_0$. Furthermore, it can be shown that a complex $S\alpha S$ random measure M_α is isotropic if and only if its circular control measure is of the form $k = m \cdot \gamma$, where γ is the uniform probability measure on S^1 [40, Example 6.1.6]. Consequently, the measure M_α and therefore the process X are uniquely characterized by control measure m .

2.1. Stationary real harmonizable $S\alpha S$ processes with finite control measure

The stochastic processes $X = \{X(t) : t \in \mathbb{R}\}$ with

$$X(t) = Re \left(\int_{\mathbb{R}} e^{itx} M_\alpha(dx) \right), \quad (2)$$

where M_α is a complex isotropic $S\alpha S$ random measure on $(\mathbb{R}, \mathcal{B})$ with finite control measure m , is called a *stationary real harmonizable $S\alpha S$ process*. The isotropy of the random measure M_α is a sufficient and necessary condition for the stationarity of the process X [40, Theorem 6.5.1], hence the control measure m uniquely determines M_α . In particular, the distribution of the process X is fully characterized by m . Indeed, it holds that the finite-dimensional characteristic function of X for all $n \in \mathbb{N}$, $s_1, \dots, s_n \in \mathbb{R}$ and $t_1, \dots, t_n \in \mathbb{R}$ is given by

$$\mathbb{E} \left[\exp \left\{ i \sum_{i=1}^n s_i X(t_i) \right\} \right] = \exp \left\{ -\lambda_\alpha \int_{\mathbb{R}} \left| \sum_{j,k=1}^n s_j s_k \cos((t_k - t_j)x) \right|^{\alpha/2} m(dx) \right\} \quad (3)$$

with constant $\lambda_\alpha = \frac{1}{2\pi} \int_0^{2\pi} |\cos(x)|^\alpha dx$ [40, Proposition 6.6.3].

Assume that the control measure m is absolutely continuous with respect to the Lebesgue measure on \mathbb{R} , i.e. it holds that $m(dx) = f(x)dx$. We refer to the Radon-Nikodym derivative f as the *spectral density* of the measure M_α (or equivalently of the process X). Clearly, under this assumption the spectral density uniquely characterizes the process X as can be seen from the finite-dimensional characteristic function of X in Equation (3). The main goal is to estimate the spectral density from a single path of X .

Statistical inference on stationary real harmonizable $S\alpha S$ processes is by far not trivial due to their non-ergodic nature. Note that the class of stationary harmonizable $S\alpha S$ processes and stationary $S\alpha S$ moving averages is disjoint for $0 < \alpha < 2$ [40, Theorem 6.7.2], see also [12] for an in-depth account on the harmonizable and moving average representation of stationary stable processes as well as [37] for details on their general structure. In fact, only in the Gaussian case ($\alpha = 2$) a stationary $S\alpha S$ process might admit both a harmonizable as well as a moving average representation.

For $0 < \alpha < 2$ the crucial difference between both classes lies in their ergodicity. In fact, stationary $S\alpha S$ moving averages are ergodic whereas stationary harmonizable $S\alpha S$ processes are non-ergodic [13]. When a stationary stochastic process is non-ergodic, the use of standard estimation methods involving empirical averages is not feasible as the limit is random. This is due to Birkhoff's ergodic theorem [22, Corollary 10.9], see also Appendix A for brief account on the ergodicity of stationary real processes.

2.2. Problem setting

The following problem can be stated for random fields on \mathbb{R}^d . For numerical reasons we stick to the one-dimensional case $d = 1$, see Remark 2. Extending the results of [21], the main focus of this work is the statistical inference on harmonizable $S\alpha S$ processes similar to Equation (2) with an *infinite control measure*, i.e. when $m(\mathbb{R}) = \infty$. If the control measure m is absolutely continuous with respect to the Lebesgue measure on \mathbb{R} , then this means that the spectral density $f(x) = m(dx)/dx$ is not integrable on \mathbb{R} .

First, note that the process

$$X(t) = \operatorname{Re} \left(\int_{\mathbb{R}} e^{itx} M_\alpha(dx) \right), \quad t \in \mathbb{R},$$

is not well defined when M_α has infinite control measure since

$$\int_{\mathbb{R}} |e^{itx}|^\alpha m(dx) = \int_{\mathbb{R}} m(dx) = m(\mathbb{R}) = \infty.$$

and the necessary condition $e^{itx} = h_t(x) \in L^\alpha(\mathbb{R}, m)$ is not fulfilled. Instead, we may consider harmonizable $S\alpha S$ processes of the form

$$X(t) = \operatorname{Re} \left(\int_{\mathbb{R}} (e^{itx} - 1) M_\alpha(dx) \right), \quad (4)$$

where again M_α is an isotropic complex $S\alpha S$ random measure with infinite control measure $m(dx) = f(x)dx$. A sufficient condition for X to be well-defined is that the spectral density f lies in the weighted Lebesgue space $L^1(\mathbb{R}, \min(1, |x|^\alpha)dx)$. This follows from the simple fact that $|e^{itx} - 1|^\alpha = 2|\sin(tx/2)|^\alpha$, which is bounded for all $t, x \in \mathbb{R}$ and behaves like $|x|^\alpha$ as $x \rightarrow 0$ for any $t \in \mathbb{R}$. Again, the goal here is to estimate the index of stability α as well as the spectral density f from a single path of X .

Alternatively, when the control measure m is the Lebesgue measure on \mathbb{R} , statistical inference for the spectral density is obviously not of interest as $f \equiv 1$. In this case, we study the class of stationary-increment harmonizable $S\alpha S$ motion $X = \{X(t) : t \in \mathbb{R}\}$ defined by

$$X(t) = \operatorname{Re} \left(\int_{\mathbb{R}} (e^{itx} - 1) \Psi(x) M_\alpha(dx) \right), \quad t \in \mathbb{R}, \quad (5)$$

where M_α is a complex isotropic $S\alpha S$ random measure with Lebesgue control measure $m(dx) = dx$ on \mathbb{R} . Here, the function Ψ is a real valued function belonging to the weighted Lebesgue space $L^\alpha(\mathbb{R}, \min(1, |x|^\alpha)dx)$ [2]. Aside from the index of stability α , the function Ψ is the new estimation target, as it uniquely defines the process X .

For both processes (4) and (5), the estimation of the spectral density f or the function Ψ , respectively, is essentially the same problem as $\widetilde{M}_\alpha(dx) = \Psi(x)M_\alpha(dx)$ is a complex, isotropic and $S\alpha S$ with control measure $\widetilde{m}(dx) = |\Psi(x)|^\alpha m(dx)$, compare [40, Proposition 3.5.5].

In some cases the function Ψ in (5) is (assumed to be) explicitly known. For $\Psi(x) = |x|^{H-1/\alpha}$ with $H \in (0, 1)$, the process

$$X^H(t) = \operatorname{Re} \left(\int_{\mathbb{R}} (e^{itx} - 1) |x|^{-H-1/\alpha} M_\alpha(dx) \right), \quad t \in \mathbb{R},$$

defines the so-called *real harmonizable fractional stable motion* [40, Section 7.7]. In the Gaussian case $\alpha = 2$, the process is the well-known fractional Brownian motion, which admits both a moving average as well as a harmonizable representation. The generalization of the harmonizable representation to the case $\alpha \in (0, 2)$ is the aforementioned harmonizable fractional stable motion, whereas the generalization of its moving average representation to $\alpha \in (0, 2)$ yields the class of linear fractional stable motions [40, Section 7.4].

The main goal here is to estimate the index of stability α and the parameter H from a single path of X^H . Similar to the Gaussian case, we refer to the parameter H as the *Hurst parameter* of the process X^H .

3. Mollifier

Let $X = \{X(t) : t \in \mathbb{R}\}$ be a measurable stationary-increment harmonizable $S\alpha S$ motion with

$$X(t) = \operatorname{Re} \left(\int_{\mathbb{R}} (e^{itx} - 1) \Psi(x) M_\alpha(dx) \right), \quad t \in \mathbb{R},$$

where M_α is a complex isotropic $S\alpha S$ random measure with Lebesgue control measure $m(dx) = dx$ and Ψ is a real-valued function in the weighted Lebesgue space $L^\alpha(\mathbb{R}, \min(1, |x|^\alpha)dx)$. If $X(t)$ is almost surely integrable with respect to $\nu(t)dt$, we define the *mollified process* $\tilde{X}_\nu = \{\tilde{X}_\nu(s) : s \in \mathbb{R}\}$ by

$$\tilde{X}_\nu(s) = \int_{\mathbb{R}} X(t)\nu(t-s)dt, \quad s \in \mathbb{R}. \quad (6)$$

For the ease of notation, we write $\tilde{X} = \tilde{X}_\nu$ in the following.

The objective of this section is to analyze the distributional behavior of the mollified process \tilde{X} as well as specifying conditions on ν for \tilde{X} to be well-defined. Indeed, it can be shown that for a suitable choice of a smoothing kernel ν the smoothed process \tilde{X} is a stationary real harmonizable stable process with finite control measure.

First, we define the Fourier transform and the inverse Fourier transform on the space of integrable and square-integrable functions on \mathbb{R} as follows. Let $\nu, w \in L^1(\mathbb{R}) \cap L^2(\mathbb{R})$. Then,

$$\mathcal{F}\nu(x) = \int_{\mathbb{R}} e^{itx}\nu(t)dt, \quad \mathcal{F}^{-1}w(t) = \frac{1}{2\pi} \int_{\mathbb{R}} e^{-itx}w(x)dx.$$

We denote by $W^{k,p}(\mathbb{R})$ the Sobolev space

$$W^{k,p}(\mathbb{R}) = \left\{ u \in L^p(\mathbb{R}) : u^{(j)} \in L^p(\mathbb{R}), j = 1, \dots, k \right\}.$$

It is well-known that the smoothness of a function and the rate of decay of its Fourier transform at the tails are directly related. In particular, it holds that $t^k \mathcal{F}u(t) \rightarrow 0$ as $|t| \rightarrow \infty$ if $u \in W^{1,k}(\mathbb{R})$. This is a direct consequence of the fact that the Fourier transform of the k -th derivative $u^{(k)}$ of a function u is given by $\mathcal{F}u^{(k)}(t) = i^k t^k \mathcal{F}u(t)$, which vanishes at its tails by the Riemann-Lebesgue lemma [18, Propositions 2.2.11(9), 2.2.17].

The following result states that under a suitable choice of the mollifier ν , the mollified process \tilde{X}_ν is a stationary real harmonizable $S\alpha S$ with finite control measure. Its proof (given in Appendix B) hinges on integrability conditions for the paths of α -stable processes given in [38] and so-called α -sine transforms.

Theorem 1. *Let $w \in L^1(\mathbb{R}) \cap L^2(\mathbb{R})$ be an even function that vanishes at 0 with $w(x) = O(|x|)$ as $|x| \rightarrow 0$. Additionally, assume that w lies in the space $W^{1,3}(\mathbb{R})$. Denote by $\nu = \mathcal{F}^{-1}w$ the Fourier inverse of w . Then, for a measurable stationary increment harmonizable $S\alpha S$ motion (5), $\alpha \in (0, 2)$, it holds that*

$$\int_{\mathbb{R}} |X(t)|\nu(t)dt < \infty \quad a.s. \quad (7)$$

Furthermore, the mollified process $\tilde{X}_\nu = \{\tilde{X}_\nu(s) : s \in \mathbb{R}\}$ is a stationary real harmonizable $S\alpha S$ process with finite control measure

$$\tilde{m}(dx) = |w(x)\Psi(x)|^\alpha dx.$$

Remark 1. One might introduce a tuning parameter $\theta > 0$ which scales the smoothing function ν by $\nu(\theta \cdot)$ such that the mollified process $\tilde{X}_{\nu,\theta} = \{\tilde{X}_{\nu,\theta}(s) : s \in \mathbb{R}\}$ is given by

$$\tilde{X}_{\nu,\theta}(s) = \int_{\mathbb{R}} X(t)\nu(\theta(t-s))dt.$$

By the scaling property of the Fourier transform, i.e. $\mathcal{F}v(\theta \cdot)(x) = \mathcal{F}v(x/\theta)/\theta = w(x/\theta)/\theta$, this directly translates to the control measure \tilde{m}_θ as

$$\tilde{m}_\theta(dx) = \left| \frac{1}{\theta} w\left(\frac{x}{\theta}\right) \Psi(x) \right|^\alpha dx.$$

4. Statistical inference

Throughout this section the following notation is used. Denote by $\tilde{X}_\theta = \tilde{X}_{v,\theta}$ the mollified process $\tilde{X}_\theta(s) = \int_{\mathbb{R}} X(t)v(\theta(t-s))dt$ with smoothing function v and scaling parameter $\theta > 0$. By Remark 1, the control measure of \tilde{X}_θ is given by $\tilde{m}_\theta(dx) = \tilde{f}_\theta(x)dx$ with the spectral density

$$\tilde{f}_\theta(x) = \left| \frac{1}{\theta} w\left(\frac{x}{\theta}\right) \Psi(x) \right|^\alpha \in L^1(\mathbb{R}).$$

Let ρ_θ be the probability density function of the underlying random frequencies $\{Z_k\}_{k=1}^\infty$ in the process' series representation with

$$\rho_\theta = \tilde{f}_\theta \left(\int_{\mathbb{R}} \tilde{f}_\theta(x) dx \right)^{-1}.$$

Choose $w \in L^1(\mathbb{R}) \cap L^2(\mathbb{R})$ to be a non-negative, even and continuous function on \mathbb{R} , and denote $w_\theta(\cdot) = w(\cdot/\theta)/\theta$. It follows that

$$\rho_\theta = w_\theta^\alpha |\Psi|^\alpha c_{\alpha,\theta}, \quad (8)$$

where $c_{\alpha,\theta} = \left(\int_{\mathbb{R}} w_\theta^\alpha(x) \Psi^\alpha(x) dx \right)^{-1}$. Additionally, assume that the function Ψ is even and continuous.

4.1. Periodogram frequency estimation for stationary real harmonizable $S\alpha S$ processes

Any stationary real harmonizable $S\alpha S$ process $\tilde{X} = \{\tilde{X}(t) : t \in \mathbb{R}\}$ with control measure $\tilde{m}(dx) = \tilde{f}(x)dx$ (and spectral density \tilde{f}) admits the LePage-type series representation

$$\tilde{X}(t) \stackrel{d}{=} C_\alpha \tilde{m}(\mathbb{R})^{1/\alpha} \sum_{k=1}^{\infty} \Gamma_k^{-1/\alpha} \left(G_k^{(1)} \cos(tZ_k) + G_k^{(2)} \sin(tZ_k) \right), \quad t \in \mathbb{R}, \quad (9)$$

where $\{\Gamma_k\}_{k \in \mathbb{N}}$ are the arrival times of a unit rate Poisson process, $\{G_k^{(j)}\}_{k \in \mathbb{N}}$, $j = 1, 2$, are sequences of i.i.d. standard normal random variables, $\{Z_k\}_{k \in \mathbb{N}}$, is a sequence of i.i.d. random variables with probability density function $\rho(\cdot) = \tilde{f}(\cdot) / \int_{\mathbb{R}} \tilde{f}(x) dx$, and

$$C_\alpha = \left(2^{\alpha/2} \Gamma\left(1 + \frac{\alpha}{2}\right) \int_0^\infty \frac{\sin(x)}{x^\alpha} dx \right)^{-1/\alpha}.$$

All sequences of random variables above are independent of each other. In particular, conditionally on $\{\Gamma_k\}_{k=1}^\infty$, $\{Z_k\}_{k=1}^\infty$, the process \tilde{X} is Gaussian with purely atomic spectral measure concentrated at the points $\{\pm|Z_k|\}_{k=1}^\infty$, cf [40, Proposition 6.6.4], which leads to the following approach.

A well-known estimation tool in spectral analysis of stationary processes is the so-called periodogram. The *periodogram* $I(\theta)$ of the sample $(x(1), \dots, x(n)) = (\tilde{X}(t_1), \dots, \tilde{X}(t_n))$ with

equidistant sample points $t_k = k\delta$, $k = 1, \dots, n$ and $\delta > 0$, from a single path of \tilde{X} as in (9) is defined by

$$I_n(\theta_j) = n^{-2} \left| \sum_{k=1}^n x(k) e^{-ik\theta_j} \right|^2,$$

where $\{\theta_j\}_{j=1}^n = \{2\pi j/n\}_{j=1}^n$ are the so-called Fourier frequencies. Straightforward computation yields that for any fixed $k \in \mathbb{N}$ the periodogram behaves like

$$I_n(\delta\theta) = \frac{R_k^2}{4} \frac{\sin^2\left(\frac{n}{2}\delta(|Z_k| - \theta)\right)}{n^2 \sin^2\left(\frac{1}{2}\delta(|Z_k| - \theta)\right)} + O(n^{-2})$$

as $\theta \rightarrow |Z_k|$ and $n \rightarrow \infty$, where

$$R_k = C_\alpha \tilde{m}(\mathbb{R})^{1/\alpha} \Gamma_k^{-1/\alpha} \sqrt{(G_k^{(1)})^2 + (G_k^{(2)})^2} \quad (10)$$

are referred to as amplitudes and Z_k as frequencies of \tilde{X} , see [21, Theorem 2]. It follows that the periodogram shows pronounced peaks at the frequencies close to the absolute frequencies $|Z_k|$.

Assuming that the spectral density ρ is an even probability density function on \mathbb{R} , i.e. $\rho(x-) = \rho(x)$ for all $x \in \mathbb{R}$, the random frequencies Z_k are i.i.d. symmetric random variables with probability density function ρ , in particular the absolute frequencies $|Z_k|$ are i.i.d. with probability density function $2\rho(x)$, $x \geq 0$.

Let $\{\hat{Z}_{N,n}\}_{k=1}^N$ be the locations of the N largest peaks of the periodogram I_n (computed as in [21, Section 4]). In addition, let $R_{[k]}$ be the amplitudes in descending order, i.e. $R_{[1]} > R_{[2]} > \dots$ a.s., and denote by $Z_{[k]}$ the corresponding frequencies. It can be shown that $\{\hat{Z}_{N,n}\}_{k=1}^N$ are strongly consistent estimators for $\{|Z_{[k]}\}_{k=1}^N$ [21, Theorem 4]. Ultimately, the kernel density estimator

$$\hat{\rho}^{(N,n)}(x) = \frac{1}{2Nh_N} \sum_{k=1}^N \kappa\left(\frac{x - \hat{Z}_{k,n}}{h_N}\right) \quad (11)$$

with kernel function κ and bandwidth h_N yields an estimate for the spectral density f on the positive real line. Under minor assumptions on ρ , κ and $\{h_N\}_{N \in \mathbb{N}}$ the pointwise and uniform consistency of $\hat{\rho}_{N,n}$ in the weak and strong sense can be established [21, Corollary 2].

Lemma 1. *Let κ be a Lipschitz-continuous kernel function and $h_N \rightarrow 0$ with $Nh_N \rightarrow \infty$. Then, for any $\varepsilon > 0$ it holds that*

$$\lim_{N \rightarrow \infty} \lim_{n \rightarrow \infty} \mathbb{P}\left(|\hat{\rho}^{(N,n)}(z) - \rho(z)| > \varepsilon\right) = 0$$

for every continuity point $z \in \mathbb{R}$ of ρ .

Remark 2. All processes introduced in Section 2.2 can be extended to random fields on \mathbb{R}^d , $d \geq 2$ by setting $(E, \mathcal{E}) = (\mathbb{R}^d, \mathcal{B}(\mathbb{R}^d))$ and replacing all products tx , $t, x \in \mathbb{R}$ by scalar products (t, x) , $t, x \in \mathbb{R}^d$, in the definitions of Section 2. The periodogram of a sample from a stationary real harmonizable $S\alpha S$ random field shows peaks corresponding to the frequencies $\mathbf{Z}_k = (Z_{k,1}, \dots, Z_{k,d})$ in all orthants of the Euclidean space \mathbb{R}^d at $(\epsilon_1 Z_{k,1}, \dots, \epsilon_d Z_{k,d})$, where $\epsilon_k = \pm 1$ for all $k = 1, \dots, d$. Hence, analogous to the symmetry condition in the one-dimensional case, the spectral density $\Psi : \mathbb{R}^d \rightarrow \mathbb{R}$ must satisfy $\Psi(x_1, \dots, x_d) = \Psi(\epsilon_1 x_1, \dots, \epsilon_d x_d)$ for all $x \in \mathbb{R}^d$ and $\epsilon_k = \pm 1$, $k = 1, \dots, d$. In practice, computational expenses for the multidimensional discrete Fourier transform, on which the periodogram relies, increase drastically with higher dimensions. For this reason, we only consider the case $d = 1$ in this work.

4.2. Stationary-increment harmonizable $S\alpha S$ motions

We consider the stationary-increment harmonizable $S\alpha S$ motion

$$X(t) = \operatorname{Re} \left(\int_{\mathbb{R}} (e^{itx} - 1) \Psi(x) M_{\alpha}(dx) \right), \quad t \in \mathbb{R},$$

where $\Psi \in L^{\alpha}(\mathbb{R}, \min(1, |x|^{\alpha})dx)$ and M_{α} is a complex, isotropic $S\alpha S$ random measure with Lebesgue control measure $m(dx) = dx$. Let $\theta_1, \theta_2 > 0$. Note that for all $z \in \mathbb{R}$ for which the ratio $\rho_{\theta_1}(z)/\rho_{\theta_2}(z)$ is well defined, it is also independent of $\Psi(x)$, in particular, by (8)

$$\frac{\rho_{\theta_1}(z)}{\rho_{\theta_2}(z)} = \frac{c_{\alpha, \theta_1} w_{\theta_1}^{\alpha}(z)}{c_{\alpha, \theta_2} w_{\theta_2}^{\alpha}(z)}. \quad (12)$$

Moreover, if w is an even, continuous function then so is $\rho_{\theta_1}/\rho_{\theta_2}$, hence it suffices to consider the positive real line only.

Consider $z_1, \dots, z_L > 0$, $L \in \mathbb{N}$. Applying a logarithmic transformation to Equation (12) yields

$$y_l = \log \left(\frac{\rho_{\theta_1}(z_l)}{\rho_{\theta_2}(z_l)} \right) = \log \left(\frac{c_{\alpha, \theta_1}}{c_{\alpha, \theta_2}} \right) + \alpha \log \left(\frac{w_{\theta_1}(z_l)}{w_{\theta_2}(z_l)} \right) = b + \alpha x_l, \quad l = 1, \dots, L. \quad (13)$$

Let $(x_{\theta_i, 1}, \dots, x_{\theta_i, n}) = (\tilde{X}_{\theta_i}(s_1), \dots, \tilde{X}_{\theta_i}(s_n))$, $i = 1, 2$, be samples of the mollified processes \tilde{X}_{θ_i} , $i = 1, 2$, sampled at equidistant points $s_j = j\delta$, $j = 1, \dots, n$, $n \in \mathbb{N}$, and $\delta > 0$. Similar to Equation (11), the kernel density type estimator $\hat{\rho}_{\theta_i}$ for ρ_{θ_i} is given by

$$\hat{\rho}_{\theta_i}^{(N, n)}(z) = \frac{1}{2Nh_N} \sum_{k=1}^N \kappa \left(\frac{z - \hat{Z}_{\theta_i, k, n}}{h_N} \right), \quad z \in \mathbb{R},$$

where $\{\hat{Z}_{\theta_i, k, n}\}_{k=1}^N$, $N \in \mathbb{N}$, $i = 1, 2$, are the periodogram frequency estimators attained from the sample of \tilde{X}_{θ_i} as described above.

Define target vectors $\mathbf{Y}_L, \hat{\mathbf{Y}}_L^{(N, n)} \in \mathbb{R}^L$ and the design matrix $\mathbf{X}_L \in \mathbb{R}^{L \times 2}$ by

$$\mathbf{Y}_L = \begin{pmatrix} \log(\rho_{\theta_1}(z_1)) - \log(\rho_{\theta_2}(z_1)) \\ \vdots \\ \log(\rho_{\theta_1}(z_L)) - \log(\rho_{\theta_2}(z_L)) \end{pmatrix}, \quad \hat{\mathbf{Y}}_L^{(N, n)} = \begin{pmatrix} \log(\hat{\rho}_{\theta_1}^{(N, n)}(z_1)) - \log(\hat{\rho}_{\theta_2}^{(N, n)}(z_1)) \\ \vdots \\ \log(\hat{\rho}_{\theta_1}^{(N, n)}(z_L)) - \log(\hat{\rho}_{\theta_2}^{(N, n)}(z_L)) \end{pmatrix},$$

and

$$\mathbf{X}_L = \begin{pmatrix} 1 & \log(w_{\theta_1}(z_1)) - \log(w_{\theta_2}(z_1)) \\ \vdots & \vdots \\ 1 & \log(w_{\theta_1}(z_L)) - \log(w_{\theta_2}(z_L)) \end{pmatrix}.$$

Then, the system of linear equations (13) generates a linear regression model written in matrix form as $\mathbf{Y}_L = \mathbf{X}_L \boldsymbol{\beta} + \boldsymbol{\varepsilon}_L$, where $\boldsymbol{\beta} = (b, \alpha)^T$ and $\boldsymbol{\varepsilon}_L$ is a vector of possible computation errors with mean vector $\mathbb{E}[\boldsymbol{\varepsilon}_L] = \mathbf{0}$ and covariance matrix $\mathbf{Q}_L = \operatorname{Cov}(\boldsymbol{\varepsilon}_L)$.

Remark 3. Consistency of the least-squares estimator $\hat{\boldsymbol{\beta}}_L = (\mathbf{X}_L^T \mathbf{X}_L)^{-1} \mathbf{X}_L^T \mathbf{Y}_L$ in a linear regression model $\mathbf{Y}_L = \mathbf{X}_L \boldsymbol{\beta} + \boldsymbol{\varepsilon}_L$ is guaranteed under the following conditions [15]. Denote by $\lambda_{\min}(\mathbf{A})$, $\lambda_{\max}(\mathbf{A})$ the smallest and largest eigenvalues of a square matrix \mathbf{A} .

If the boundary conditions $\lambda_{\max}(Q_L) < \infty$, $\lambda_{\min}(Q_L) > 0$ are fulfilled and $\lambda_{\min}(\mathbf{X}^T \mathbf{X}) \rightarrow \infty$ as $L \rightarrow \infty$, then the least-squares estimator $\hat{\boldsymbol{\beta}}_L$ of $\boldsymbol{\beta}$ is weakly consistent. The above is fulfilled for the usual assumptions on linear regression models, i.e. when the vector of errors $\boldsymbol{\varepsilon}$ is homoscedastic with uncorrelated components, and $L^{-1} \mathbf{X}_L^T \mathbf{X}_L$ converges to some covariance matrix Q as $L \rightarrow \infty$. Additionally, conditions for strong consistency are given in [15, Section 4].

Consider z_1, \dots, z_L , $L \in \mathbb{N}$, such that $w_{\theta_1}(z_i)/w_{\theta_2}(z_i) \neq w_{\theta_1}(z_j)/w_{\theta_2}(z_j)$ for some $i \neq j$. This ensures that the matrix $\mathbf{X}^T \mathbf{X}$ is invertible and its eigenvalues λ_1, λ_2 can be computed explicitly, i.e.

$$\lambda_{1,2} = \frac{1}{2} \left(L + \sum_{l=1}^L x_l^2 \pm \sqrt{\left(L + \sum_{l=1}^L x_l^2 \right)^2 - 4 \left(L \sum_{l=1}^L x_l^2 - \left(\sum_{l=1}^L x_l \right)^2 \right)} \right),$$

where $x_l = \log(w_{\theta_1}(z_l)/w_{\theta_2}(z_l))$, $l = 1, \dots, L$. It is easy to verify that $\lambda_{\min}(\mathbf{X}^T \mathbf{X}) \rightarrow \infty$ as $L \rightarrow \infty$.

Denote by $\boldsymbol{\beta}_L^{(N,n)} = (\hat{b}_L^{(N,n)}, \hat{\alpha}_L^{(N,n)})^T$ the least-squares estimator for $\boldsymbol{\beta}$ in the linear regression model $\hat{\mathbf{Y}}_L^{(N,n)} = \mathbf{X}_L \boldsymbol{\beta} + \boldsymbol{\varepsilon}_L$, i.e.

$$\boldsymbol{\beta}_L^{(N,n)} = (\hat{b}_L^{(N,n)}, \hat{\alpha}_L^{(N,n)})^T = (\mathbf{X}_L^T \mathbf{X}_L)^{-1} \mathbf{X}_L^T \hat{\mathbf{Y}}_L^{(N,n)}.$$

Corollary 1. Let the kernel density estimators $\hat{\rho}_{\theta_i}^{(N,n)}$, $i = 1, 2$, satisfy the conditions of Lemma 1. Assume that the conditions on the error vector $\boldsymbol{\varepsilon}_L$ in Remark 3 are fulfilled. Then, the least-squares estimator $\boldsymbol{\beta}_L^{(N,n)}$ is consistent for $\boldsymbol{\beta}$ in the sense that

$$\lim_{L \rightarrow \infty} \lim_{N \rightarrow \infty} \lim_{n \rightarrow \infty} \mathbb{P}(|\hat{b}_L^{(N,n)} - b| > \varepsilon) = 0, \quad \lim_{L \rightarrow \infty} \lim_{N \rightarrow \infty} \lim_{n \rightarrow \infty} \mathbb{P}(|\hat{\alpha}_L^{(N,n)} - \alpha| > \varepsilon) = 0. \quad (14)$$

Proof. The full rank of $\mathbf{X}^T \mathbf{X}$ is ensured by the choice of z_1, \dots, z_L , thus the linear least-squares minimization has a unique solution $(b, \alpha)^T$. Note that in the following when referring to consistency of $\hat{\rho}_{\theta_i}^{(N,n)}$, we always consider the double limits in the order $\lim_{N \rightarrow \infty} \lim_{n \rightarrow \infty}$. Under the conditions of Lemma 1 the estimators $\hat{\rho}_{\theta_i}^{(N,n)}$, $i = 1, 2$, are weakly pointwise consistent at z_1, \dots, z_L . Hence, it follows that $\hat{\mathbf{Y}}^{(N,n)}$ is weakly consistent for \mathbf{Y} by the continuous mapping theorem, and

$$\hat{\boldsymbol{\beta}}_L^{(N,n)} = (\mathbf{X}_L^T \mathbf{X}_L)^{-1} \mathbf{X}_L^T \hat{\mathbf{Y}}_L^{(N,n)} \xrightarrow{P} (\mathbf{X}_L^T \mathbf{X}_L)^{-1} \mathbf{X}_L^T \mathbf{Y}_L =: \hat{\boldsymbol{\beta}}_L$$

as first $n \rightarrow \infty$, then $N \rightarrow \infty$. By the triangle inequality

$$|\hat{\boldsymbol{\beta}}_L^{(N,n)} - \boldsymbol{\beta}| \leq |\hat{\boldsymbol{\beta}}_L^{(N,n)} - \hat{\boldsymbol{\beta}}_L| + |\hat{\boldsymbol{\beta}}_L - \boldsymbol{\beta}|$$

Equations (14) follows. \square

Remark 4. If ρ_{θ} is known to be uniformly continuous and $Nh_N^2 \rightarrow \infty$ holds, then

$$\lim_{N \rightarrow \infty} \lim_{n \rightarrow \infty} \mathbb{P}(\|\hat{\rho}_{\theta}^{(N,n)} - \rho_{\theta}\|_{\infty} > \varepsilon) = 0.$$

Furthermore, strong uniform consistency

$$\mathbb{P}\left(\lim_{N \rightarrow \infty} \lim_{n \rightarrow \infty} \|\hat{\rho}_\theta^{(N,n)} - \rho_\theta\|_\infty = 0\right) = 1$$

is ensured if, additionally to its Lipschitz-continuity as in Lemma 1, the kernel function κ has bounded variation, vanishes at $\pm\infty$ and the bandwidth satisfies $\sum_{N=1}^{\infty} \exp(-rNh_N^2) < \infty$ for any $r > 0$, cf. [21] By the same arguments as above this yields strong consistency of $(\hat{b}^{(N,n)}, \hat{a}^{(N,n)})^T$ for $(b, \alpha)^T$.

Note that, a consistent estimator for $c_{\alpha,\theta}\Psi^\alpha$, i.e. an estimator for the function Ψ^α up to a constant factor, is given by $(\hat{\rho}_\theta^{(N,n)})_{w_\theta^{-\hat{a}^{(N,n)}}}$. Pointwise and uniform consistency in the weak and strong sense can be accomplished by Corollary 1 and Remark 4 under the respective conditions.

Remark 5. The kernel function Ψ can only be restored from the random frequencies $\{Z_k\}_{k=1}^\infty$ up to a constant multiplicative factor. Consider the scaled version X_c , $c > 0$, of a stationary-increment harmonizable stable process X with

$$X_c(t) = \operatorname{Re} \left(\int_{\mathbb{R}} (e^{itx} - 1) c\Psi(x) M_\alpha(dx) \right), \quad t \in \mathbb{R}.$$

Then, the mollified process $\tilde{X}_{c,\theta}(s) = \int_{\mathbb{R}} X_c(t) \nu(\theta(t-s)) dt$ is a stationary real harmonizable $S\alpha S$ process with finite control measure $\tilde{m}_{c,\theta}(dx) = c^\alpha w_\theta^\alpha(x) |\Psi(x)|^\alpha dx$. The underlying i.i.d. random frequencies $\{Z_k\}_{k=1}^\infty$ in the corresponding LePage series representation, upon which all estimates rely, are independent of the constant c , since it cancels in their probability density function

$$\rho_{c,\theta}(x) = c^\alpha w_\theta^\alpha(x) |\Psi(x)|^\alpha \left(\int_{\mathbb{R}} c^\alpha w_\theta^\alpha(x) |\Psi(x)|^\alpha dx \right)^{-1} = w_\theta^\alpha(x) |\Psi(x)|^\alpha \left(\int_{\mathbb{R}} w_\theta^\alpha(x) |\Psi(x)|^\alpha dx \right)^{-1}.$$

4.3. Real harmonizable fractional stable motions

We apply the results of Section 3 to the class of real harmonizable fractional stable motions $X^H = \{X^H(t) : t \in \mathbb{R}\}$ given by

$$X^H(t) = \operatorname{Re} \left(\int_{\mathbb{R}} (e^{itx} - 1) |x|^{-H-1/\alpha} M_\alpha(dx) \right),$$

where $\alpha \in (0, 2)$, $H \in (0, 1)$ and M_α is a complex isotropic $S\alpha S$ random measure with Lebesgue control measure $m(dx) = dx$. The additional pre-knowledge of $\Psi(x) = |x|^{-H-1/\alpha}$ allows us to propose an estimation procedure, which is explicitly tailored to real harmonizable fractional stable motions.

Corollary 2. Let $w, v \in L^1(\mathbb{R}) \cap L^2(\mathbb{R})$ be even functions given by $w(x) = |x|^p e^{-|x|^q}$, $p, q \geq 1$, and $v = \mathcal{F}^{-1}w$.

- (i) The mollified process $\tilde{X}_\theta = \{\tilde{X}_\theta(s) : s \in \mathbb{R}\}$ with $\tilde{X}_\theta(s) = \int_{\mathbb{R}} X^H(t) \nu(\theta(t-s)) dt$, $s \in \mathbb{R}$, $\theta > 0$, is a stationary real harmonizable $S\alpha S$ process with finite control measure \tilde{m}_θ . The random frequencies $\{Z_k\}_{k \in \mathbb{N}}$ in its LePage series representation (9) are i.i.d. with probability density function

$$\rho_\theta(z) = \frac{q}{2} \frac{(\alpha\theta^{-q})^{\frac{\alpha}{q}(p-H)}}{\Gamma\left(\frac{\alpha}{q}(p-H)\right)} e^{-\alpha\theta^{-q}|z|^q} |z|^{\alpha(p-H)-1}, \quad z \in \mathbb{R}. \quad (15)$$

(ii) It holds that $\{|Z_k|^q\}_{k \in \mathbb{N}}$ is a sequence of i.i.d. Gamma-distributed random variables with shape parameter $\frac{\alpha}{q}(p-H)$ and scale parameter $\alpha\theta^{-q}$, i.e.

$$|Z_k|^q \sim \Gamma\left(\frac{\alpha}{q}(p-H), \alpha\theta^{-q}\right).$$

Proof. (i) The weight function w fulfills all necessary conditions of Theorem 1. It follows that $\int_{\mathbb{R}} |X^H(t)|^p dt < \infty$ a.s. and in particular the mollified process $\tilde{X} = \tilde{X}_{v,\theta}$ with

$$\tilde{X}(s) \stackrel{a.s.}{=} \int_{\mathbb{R}} e^{isx} w_{\theta}(x) |x|^{-H-1/\alpha} M_{\alpha}(dx), \quad s \in \mathbb{R},$$

is a stationary real harmonizable $S\alpha S$ process with finite control measure

$$\tilde{m}_{\theta}(dx) = \tilde{f}_{\theta}(x) dx = w_{\theta}^{\alpha}(x) |x|^{-\alpha H-1} dx.$$

Therefore, it admits the LePage series representation (9) with frequencies $\{Z_k\}_{k \in \mathbb{N}}$, which are i.i.d. with probability density function $\rho_{\theta} = \tilde{f}_{\theta} \left(\int_{\mathbb{R}} \tilde{f}_{\theta}(x) dx \right)^{-1}$.

Note that the spectral density \tilde{f} is given by

$$\tilde{f}_{\theta}(x) = w_{\theta}^{\alpha}(x) |x|^{-\alpha H-1} = \theta^{-\alpha(1+p)} e^{-\alpha\theta^{-q}|x|^q} |x|^{\alpha(p-H)-1}$$

and

$$\begin{aligned} \int_{\mathbb{R}} \tilde{f}_{\theta}(x) dx &= \theta^{-\alpha(1+p)} \int_{\mathbb{R}} e^{-\alpha\theta^{-q}|x|^q} |x|^{\alpha(p-H)-1} dx \\ &= \frac{2}{q} \theta^{-\alpha(1+p)} \frac{\Gamma\left(\frac{\alpha}{q}(p-H)\right)}{(\alpha\theta^{-q})^{\frac{\alpha}{q}(p-H)}} \underbrace{\int_0^{\infty} \frac{(\alpha\theta^{-q})^{\frac{\alpha}{q}(p-H)}}{\Gamma\left(\frac{\alpha}{q}(p-H)\right)} e^{-\alpha\theta^{-q}\eta} \eta^{\alpha - \frac{\alpha H}{q} - 1} d\eta}_{=1}, \end{aligned}$$

where we substituted $\eta = x^q$ in the above integration and expanded by the normalizing constant of the Gamma distribution with shape parameter $\frac{\alpha}{q}(p-H)$ and scale parameter $\alpha\theta^{-q}$. Consequently, this yields

$$\rho_{\theta}(z) = \frac{q}{2} \frac{(\alpha\theta^{-q})^{\frac{\alpha}{q}(p-H)}}{\Gamma\left(\frac{\alpha}{q}(p-H)\right)} e^{-\alpha\theta^{-q}|z|^q} |z|^{\alpha(p-H)-1}.$$

(ii) The sequence $\{|Z_k|^q\}_{k \in \mathbb{N}}$ consists of i.i.d. random variables. Denote their probability density function by g . By the density transformation theorem with transform $\varphi(z) = |z|^q$ we can compute

$$\begin{aligned} g(z) &= \left(\rho_{\theta}\left(-z^{\frac{1}{q}}\right) + \rho_{\theta}\left(z^{\frac{1}{q}}\right) \right) \frac{1}{q} z^{\frac{1}{q}-1} \\ &= 2 \frac{q}{2} \frac{(\alpha\theta^{-q})^{\frac{\alpha}{q}(p-H)}}{\Gamma\left(\frac{\alpha}{q}(p-H)\right)} e^{-\alpha\theta^{-q}z^{\frac{1}{q}(\alpha(p-H)-1)}} \frac{1}{q} z^{\frac{1}{q}-1} \end{aligned}$$

$$= \frac{(\alpha\theta^{-q})^{\frac{\alpha}{q}(p-H)}}{\Gamma\left(\frac{\alpha}{q}(p-H)\right)} e^{-\alpha\theta^{-q}z} z^{\frac{\alpha}{q}(p-H)-1},$$

which is the probability density function of the Gamma distribution with shape parameter $\frac{\alpha}{q}(p-H)$ and scale parameter $\alpha\theta^{-q}$. □

Applying the periodogram method described in Section 4.1 to the mollified process \tilde{X}_θ the parameters α and H can be estimated as follows. Consider the sample $(x_{\theta,1}, \dots, x_{\theta,n}) = (X_\theta(t_1), \dots, X_\theta(t_n))$ where $t_j = j\delta$, $j = 1, \dots, n$, $\delta > 0$. Denote by $\{\hat{Z}_{k,n}\}_{k=1}^N$ the periodogram frequency estimators of $\{Z_{[k]}\}_{k=1}^N$ as described in Section 4.1.

Consider an i.i.d. random sample $X_1, \dots, X_n \sim \Gamma(b, r)$, $b, r > 0$. Strongly consistent closed form estimators for the parameters (b, r) are given in [43], i.e.

$$\begin{aligned} \tilde{b}(X_1, \dots, X_N) &= \frac{N \sum_{k=1}^N X_k}{N \sum_{k=1}^N X_k \log(X_k) - \sum_{k=1}^N \log(X_k) \sum_{k=1}^N X_k}, \\ \tilde{r}(X_1, \dots, X_N) &= \frac{N^2}{N \sum_{k=1}^N X_k \log(X_k) - \sum_{k=1}^N \log(X_k) \sum_{k=1}^N X_k}. \end{aligned}$$

The index of stability α and the Hurst parameter H can therefore be estimated by

$$\begin{aligned} \tilde{\alpha}^{(N,n)} &= \theta^q \tilde{r}(\hat{Z}_{1,n}^q, \dots, \hat{Z}_{N,n}^q), \\ \tilde{H}^{(N,n)} &= p - q \frac{\tilde{b}(\hat{Z}_{1,n}^q, \dots, \hat{Z}_{N,n}^q)}{\tilde{\alpha}^{(N,n)}}. \end{aligned}$$

Corollary 3. *The estimators $(\tilde{\alpha}^{N,n}, \tilde{H}^{N,n})$ are strongly consistent for (α, H) , i.e.*

$$\mathbb{P}\left(\lim_{N \rightarrow \infty} \lim_{n \rightarrow \infty} \tilde{\alpha}^{N,n} = \alpha\right) = 1, \quad \mathbb{P}\left(\lim_{N \rightarrow \infty} \lim_{n \rightarrow \infty} \tilde{H}^{N,n} = H\right) = 1$$

Proof. The strong consistency of the periodogram frequency estimators $\{\hat{Z}_{k,n}\}_{k=1}^N$ for $\{Z_{[k]}\}_{k=1}^N$ was proven in [21, Theorem 4]. Clearly, by the continuity of the mapping $z \mapsto |z|^q$ it follows that $\{\hat{Z}_{k,n}^q\}_{k=1}^N$ are strongly consistent for $\{Z_{[k]}^q\}_{k=1}^N$, which are i.i.d. Gamma distributed with shape parameter $\alpha - \frac{\alpha H}{q}$ and rate $\alpha\theta^{-q}$ by Corollary 2 (ii). Solving for α and H and applying the continuous mapping theorem once again concludes the proof. □

The choice of the parameters $p, q \geq 1$ is discussed in Remark 6 in the next section.

5. Simulation study

In this section, we consider estimation based on a single path of a real harmonizable fractional stable motion ("real HFSM" in the following) X^H as in Section 4.3. Let $(x_1, \dots, x_n) = (X^H(t_1), \dots, X^H(t_n))$ be a sample of a single path of X^H , where the points $\{t_j\}_{j=1}^n$ are chosen equidistantly with $t_j = j\delta$, $j = 1, \dots, n$, and mesh size $\delta > 0$. The simulation is performed via the discretization of the integral representation of X^H . Realizations of X^H for $\alpha \in \{0.75, 1.5\}$ and $H \in \{0.25, 0.75\}$ are given in Figure 1 with the same simulation seed being used in each realization. As it is the case for the classical fractional Brownian motion, the Hurst parameter H determines the roughness of the paths. Additionally, the smaller the index of stability α the higher the fluctuations as well.

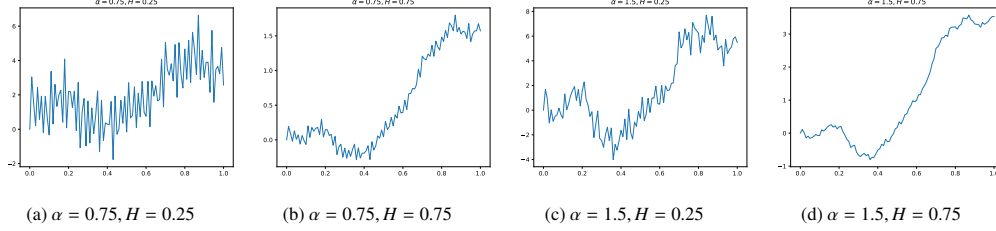


Figure 1: Realization of a real HFMSM for $\alpha \in \{0.75, 1.5\}$ and $H \in \{0.25, 0.75\}$ on $[0, 1]$. The simulations are based on the same seed to emphasize the effect of α and H on the paths' roughness.

Example 1. Consider the even weight function $w(x) = |x|^p e^{-|x|^q}$, $p, q \geq 1$ of Corollary 2. Setting the exponent $q = 2$ in the exponential term of w guarantees its (inverse) Fourier transform can be given explicitly. In particular, it holds that $v = \mathcal{F}^{-1}w$ with $w(x) = |x|^p e^{-x^2}$, $p \geq 1$, is of the form

$$v(t) = \frac{1}{2\pi} \Gamma\left(\frac{1+p}{2}\right) {}_1F_1\left(\frac{1+p}{2}; \frac{1}{2}; -\frac{t^2}{4}\right),$$

where ${}_1F_1$ is a generalized hypergeometric series defined by ${}_1F_1(a; b; z) = \sum_{n=1}^{\infty} \frac{a^{(n)} z^n}{b^{(n)} n!}$, $z \in \mathbb{C}$, and rising factorials $a^{(0)} = 1$, $a^{(n)} = a(a+1) \dots (a+n-1)$.

In particular, for $p = 2, 4$ this yields

$$w^{(1)}(x) = x^2 e^{-x^2}, \quad v^{(1)}(t) = \frac{1}{8\sqrt{\pi}} e^{-\frac{t^2}{4}} (2 - t^2) \quad (16)$$

and

$$w^{(2)}(x) = x^4 e^{-x^2}, \quad v^{(2)}(t) = \frac{1}{32\sqrt{\pi}} e^{-\frac{t^2}{4}} (12 - 12t^2 + t^4). \quad (17)$$

The choice of $p, q \geq 1$ and their effect on the asymptotic variance of the estimators \tilde{b}, \tilde{r} of the Gamma distribution are discussed in more detail in Remark 6.

We compute samples of the path of the mollified process $\tilde{X}_{v,\theta}$ via discrete convolution. Fix an even number of discretization points $L \in \mathbb{N}$ of v_θ . Recall that the function v_θ is even, hence consider its discretization $(v_{\theta,0}, \dots, v_{\theta,L})$ on the interval $[-\delta L/2, \delta L/2]$ with $v_l = v\left(\delta\left(-\frac{L}{2} + l\right)\right)$, $l = 0, \dots, L$. The convolution operation is performed only where the samples (x_0, \dots, x_n) and $(v_{\theta,0}, \dots, v_{\theta,L})$ fully overlap (in time), i.e. compute $(\tilde{x}_{\theta,0}, \dots, \tilde{x}_{\theta,n-L})$ with

$$\tilde{x}_{\theta,k} = \delta \sum_{l=0}^L x_{k-l} v_l \approx \tilde{X}_{v,\theta}\left(\delta\left(\frac{L}{2} + k\right)\right), \quad k = 0, \dots, n-L. \quad (18)$$

For the numerical computation we use Python's `scipy.signal.convolve` function and its mode parameter set to 'valid'.

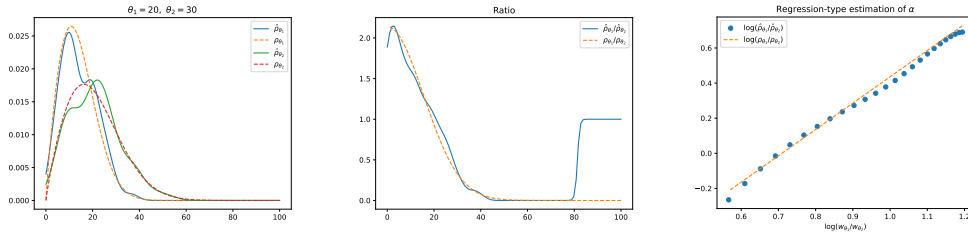
The number L should be chosen such that $n-L$ is still large enough for periodogram computations, i.e. $n-L \geq n_0$ for some desired minimal sample size n_0 . Furthermore, the tuning parameter θ should be chosen such that the discretization $(v_{\theta,0}, \dots, v_{\theta,L})$ on the points $\{\delta(-L/2 + j)\}_{j=0}^L$ approximate v_θ well enough and $|v_\theta(t)| < \varepsilon$, $t \notin [-\delta L/2, \delta L/2]$, for some small $\varepsilon > 0$. For the discretization of v_θ we set $L = 100$, $\delta = 0.01$, which yields the interval $[-0.5, 0.5]$ on which v_θ is discretized. Setting $\theta = 20$ guarantees that v_θ is negligible outside of $[-0.5, 0.5]$.

5.1. Regression based estimation of α

Figure 2 visualizes the regression based estimation of the index of stability α as described in Section 4.2. Subfigure (a) shows the true ρ_{θ_i} (dashed lines) against its estimates $\hat{\rho}_{\theta_i}$ (solid lines), $i = 1, 2$, where $\theta_1 = 20$, $\theta_2 = 30$. The estimation is based on the simulation of a single path of X^H with $(\alpha, H) = (1.5, 0.75)$ equidistant sample points with mesh size $\delta = 0.01$ and $n = 10000$. This path is then mollified twice with $v^{(1)}$ of Example 1, once with θ_1 and once with θ_2 .

Subfigure (b) shows the ratio $\hat{\rho}_{\theta_1}/\hat{\rho}_{\theta_2}$ against the true ratio $\rho_{\theta_1}/\rho_{\theta_2}$. Since it holds that $\rho_{\theta_1}/\rho_{\theta_2} = C(w_{\theta_1}/w_{\theta_2})^\alpha$, where C is a constant and $w_{\theta_1}/w_{\theta_2}$ is known, it is possible to deduce the general shape of the true ratio $\rho_{\theta_1}/\rho_{\theta_2}$. Stronger deviations from this shape such as the downward kink of $\hat{\rho}_{\theta_1}/\hat{\rho}_{\theta_2}$ near the origin and the jump at its right tail can be explained by the fact that both ρ_{θ_1} and ρ_{θ_2} vanish at the origin at their tails, combined with inaccuracy of kernel density estimation at those ends.

Before computing the log-transformed ratio of $\log(\hat{\rho}_{\theta_1}(z)/\hat{\rho}_{\theta_2}(z))$, we restrict ratio to the interval $[b_l, b_u]$, where the lower bound $b_l = 1$ was chosen to exclude fluctuations near the origin and b_u is chosen automatically such that there are no jumps at the right tail of the ratio and the ratio is larger than the threshold $\varepsilon = 0.05$. A visualization of the linear dependency in α (cf. Equation (13)) can be seen in Subfigure (c). In this example, linear regression yields the estimate $\hat{\alpha} = 1.467$.



(a) Spectral density estimation with $\theta_1 = 20$ (blue and orange) and $\theta_2 = 30$ (green and red). Dashed lines (orange and red) are the true normalized spectral densities ρ_{θ_i} , $i = 1, 2$, whereas the solid lines (blue and green) are the estimates $\hat{\rho}_{\theta_i}$, $i = 1, 2$. (b) True ratio $\rho_{\theta_1}/\rho_{\theta_2}$ (orange dashed line) and estimated ratio $\hat{\rho}_{\theta_1}/\hat{\rho}_{\theta_2}$ (blue solid line) over the interval $[0, 100]$. (c) True log-ratio $\log(\rho_{\theta_1}/\rho_{\theta_2})$ (orange dashed line) and estimated log-ratio $\log(\hat{\rho}_{\theta_1}/\hat{\rho}_{\theta_2})$ (blue dots).

Figure 2: Estimation of the index of stability α based on a single path of X^H with $\alpha = 1.5$ sampled equidistantly with $\delta = 0.01$, $n = 10000$. The dashed lines (orange and red) are the true normalized spectral densities ρ_{θ_i} , $i = 1, 2$, whereas the solid lines (blue and green) are the estimates $\hat{\rho}_{\theta_i}$, $i = 1, 2$.

In Table 1 we give the mean bias of the regression estimator computed from 1000 estimations of α based on 1000 single paths. The accuracy of the estimator increases with increasing sample size and consequently increasing number of frequencies N used for kernel density estimation. Naturally, the estimator performs better the better the kernel density estimation of ρ_{θ_i} , which is reflected by the performance in the case $\alpha = 1.5$ compared to $\alpha = 0.75$. Note that for the computation of the mean bias, estimates $\hat{\alpha} \notin (0, 2)$ were excluded, see Appendix C Table C.5. For instance in the case $\alpha = 1.5$ with smoothing by $v^{(1)}$, sample size $n = 10^4$ and number of estimated frequencies $N = 200$ the number of outliers was 38 out of 1000. Upon closer inspection, in each of those cases high fluctuations at the tail of the estimated ratio $\hat{\rho}_{\theta_1}(z)/\hat{\rho}_{\theta_2}(z)$ were the main problem. A more conservative choice of the lower bound b_l and the threshold ε or manually adjusting the bounds of the interval on which the log ratio is computed will lead to a significant improvement of the estimate $\hat{\alpha}$.

Mean bias $\hat{\alpha} - \alpha$	α	δ	0.01					
		n	10^3			10^4		
		N H	10	25	40	100	150	200
$w_{20}^{(1)}$	0.75	0.25	-0.056	0.136	-0.078	0.084	0.145	0.158
		0.75	-0.142	0.100	-0.101	0.081	0.109	0.143
	1.5	0.25	-0.338	-0.221	-0.577	-0.009	-0.001	-0.032
		0.75	-0.467	-0.208	-0.615	-0.042	-0.003	-0.032
$w_{20}^{(2)}$	0.75	0.25	0.021	0.163	0.028	0.115	0.145	0.180
		0.75	0.041	0.158	0.003	0.113	0.161	0.173
	1.5	0.25	-0.537	-0.259	-0.490	-0.161	-0.104	-0.065
		0.75	-0.483	-0.238	-0.529	-0.095	-0.045	-0.053

Table 1: Mean bias of the regression estimator $\hat{\alpha}$ to α based on the log-transformed ratio $\hat{\rho}_{\theta_1}/\hat{\rho}_{\theta_2}$ with $\theta_1 = 20$, $\theta_2 = 30$. Computations are based on 1000 single path simulations and spectral density estimation for each path. Each path is sampled equidistantly with mesh size $\delta = 0.01$ and sample size $n = 1000$ and $n = 10000$, respectively.

5.2. Analysis of the kernel density estimator $\hat{\rho}_\theta$

The results in Figure 3 are based on a single path of a real HFSM, with $(\alpha, H) = (0.75, 0.25)$ in Subfigures (a), (b) and once with $(\alpha, H) = (1.5, 0.75)$ in Subfigures (c), (d). Each path was sampled equidistantly with mesh size $\delta = 0.01$ and sample size $n = 1000$ in (a), (c) and $n = 10000$ in (b), (d). Convolution was then performed with $v^{(1)}$ of Example 1, where $L = 100$ and $\theta = 20$ resulting in the sample $\tilde{x} = (\tilde{x}_{\theta,0}, \dots, \tilde{x}_{\theta,n-L})$. Choose the number of frequencies N estimated from the periodogram of \tilde{x} such that $N^{2/5}/(n-L) \leq \varepsilon$ for some small error $\varepsilon > 0$. Here, for $n - L = 900$, we set $N = 25$ and $\varepsilon = 0.005$ for (a), (c). See [21] for a more detailed account on the choice of N .

When increasing the sample size to $n = 10000$, the relation $N^{2/5}/(n-L) \leq \varepsilon$ allows us to increase the number of frequencies to be estimated to $N = 150$, while keeping everything else unchanged. This leads to an improvement of the estimation results, see Subfigures (b) and (d). For the kernel density estimator $\hat{\rho}_\theta$ we use the Gaussian kernel function with Silverman's rule for bandwidth selection. The blue line shows the estimator $\hat{\rho}_\theta$ and the orange dashed line shows the true normalized spectral density ρ_θ of the mollified process \tilde{X}_θ .

In Table 2 we compute the mean squared L^2 -distance $\|\hat{\rho}_\theta - \rho_\theta\|_2^2$ on the interval $[0, 100]$. For this a single path of X^H with $\alpha = 0.75, 1.5$ and $H = 0.25, 0.75$ was simulated 1000 times and sampled equidistantly with mesh size $\delta = 0.01$. For the sample size we consider the cases $n = 1000$ and $n = 10000$. Each sample path is smoothed with $v^{(i)}$, $i = 1, 2$, from Example 1 and $\theta = 20$, $L = 100$. Then, N frequencies are estimated from the periodogram of the sample path of the mollified process.

We see an improvement in accuracy, the higher the sample size n and the number of frequencies N used for kernel density estimation are. The smaller the index of stability and the Hurst parameter, the more difficult the estimation of ρ . This is to be expected as the path behavior becomes more erratic with decreasing α and H . Upon further inspection we discover that the high values for the L^2 -distance appearing in particular for the cases $n = 1000$ and $\alpha = 0.75$ arise

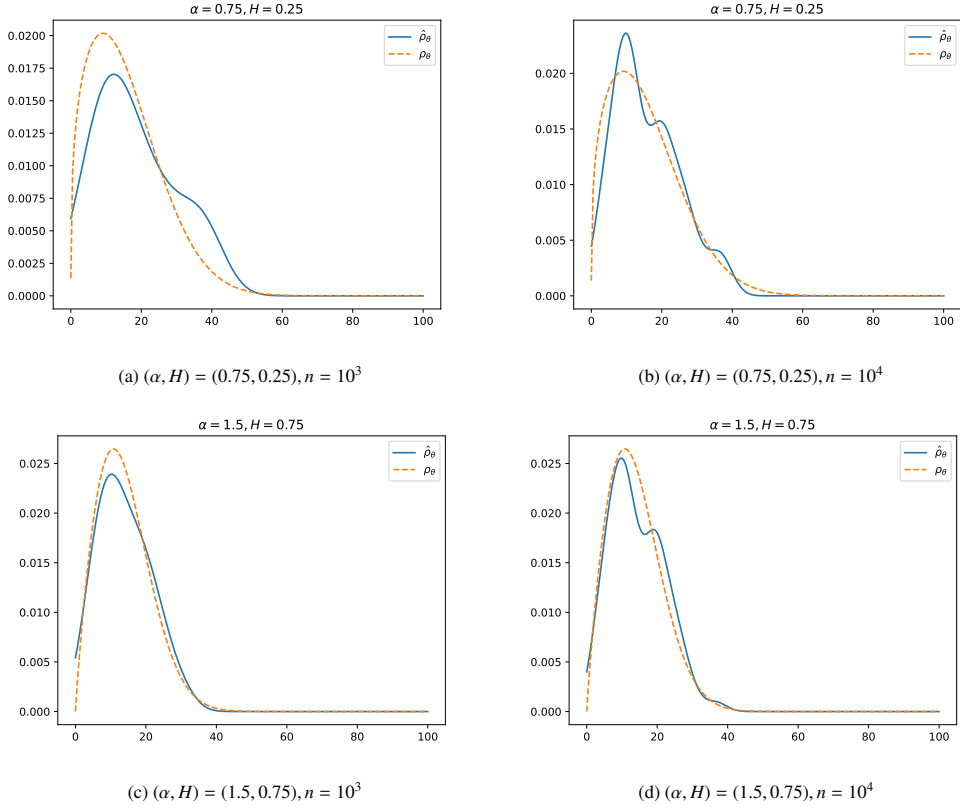


Figure 3: Spectral density estimation for the mollified process for the cases $(\alpha, H) = (0.75, 0.25)$ in Subfigures (a) and (b) as well as $(\alpha, H) = (1.5, 0.75)$ in (c) and (d), each based on a single path of a real HFSM X^H , respectively.

from outliers in the estimation of ρ . Excluding the effect of these outliers we give the median L^2 -distance under the same setting as Table 2 in Appendix C, Table C.4.

Lower accuracy of the spectral density estimation for the case $\alpha = 0.75$ compared to $\alpha = 1.5$ can be explained by the following. The deviations between ρ_θ and $\hat{\rho}_\theta$ are due to the fact that the smaller α the faster the decay of the sequence $\{\Gamma_k^{-1/\alpha}\}_{k=1}^\infty$ in the LePage series representation of \tilde{X}_θ , see Corollary 2. As a consequence, only a few amplitudes R_k , see Equation (10), dominate all the remaining amplitudes in size. Due to the nature of the discrete Fourier transform, which the periodogram is based on, the periodogram will oscillate around the frequencies corresponding to the dominating amplitudes, which leads to difficulties in the estimation of the absolute frequencies $|Z_k|$. These oscillations are also called sidelobes and are addressed in [19, 21, 36].

In particular, the case $(\alpha, H) = (0.75, 0.75)$ has the problem that the true density ρ_θ does not vanish at the origin. In general, for a real HFSM this is the case when $\alpha(p - H) - 1 < 0$, where $p \geq 1$ is the exponent in $w(x) = |x|^p e^{-|x|^q}$, which might happen if α is relatively small. Therefore, it is more likely that the random frequencies Z_k take values in a neighborhood of 0 compared to the case of ρ_θ vanishing at the origin. This can cause problems for the frequency estimation as it is hard to detect frequencies close to 0 via the periodogram [36, Chapter 3.5]. To counter this,

Mean squared L^2 -dist. $\ \hat{\rho} - \rho\ _2^2 (\times 10^{-3})$	α	δ	0.01					
		n	10^3			10^4		
		N	10	25	40	100	150	200
$w_{20}^{(1)}$	0.75	0.25	7.434	1.853	1.146	7.324	4.629	3.170
		0.75	7.687	2.656	2.690	7.662	4.866	3.493
	1.5	0.25	2.499	0.690	1.213	0.922	0.515	0.357
		0.75	2.449	0.701	1.383	0.908	0.516	0.374
$w_{20}^{(2)}$	0.75	0.25	7.670	2.276	1.185	7.546	4.943	3.564
		0.75	7.834	2.184	1.097	7.637	4.965	3.569
	1.5	0.25	2.384	0.673	1.136	0.931	0.514	0.358
		0.75	2.355	0.667	1.133	0.921	0.509	0.350

Table 2: Mean squared L^2 -distances between kernel density estimators $\hat{\rho}_\theta$ and normalized spectral density ρ_θ over the interval $[0, 100]$. Computations are based on 1000 single path simulations and spectral density estimation for each path.. Each path is sampled equidistantly with mesh size $\delta = 0.01$ and sample sizes $n = 1000$ and $n = 10000$, respectively.

consider increasing the rate of decay of w at the origin by increasing p as for example $p = 4$ in the function $w^{(2)}$, see Example 1 and the corresponding smoothing function $v^{(2)}$.

Figure 4 compares estimation results for ρ_θ based on the same path realization of X^H with $(\alpha, H) = (0.75, 0.75)$ but once mollified with $v^{(1)}$ in Subfigure (a) and once with $v^{(2)}$ in Subfigure (b). In Subfigure (a) with $p = 2$ it holds that $\rho_\theta(z) \sim |z|^{-1/4}$ as $z \rightarrow 0$, whereas in the case of Subfigure (b) we have $\rho_\theta(z) \sim |z|^{3/4}$ as $z \rightarrow 0$. In Subfigure (a) we see that the estimator $\hat{\rho}_\theta$ strongly deviates from ρ_θ close to the origin due to the aforementioned issue of small frequency estimation. This is not apparent in Subfigure (b) anymore.

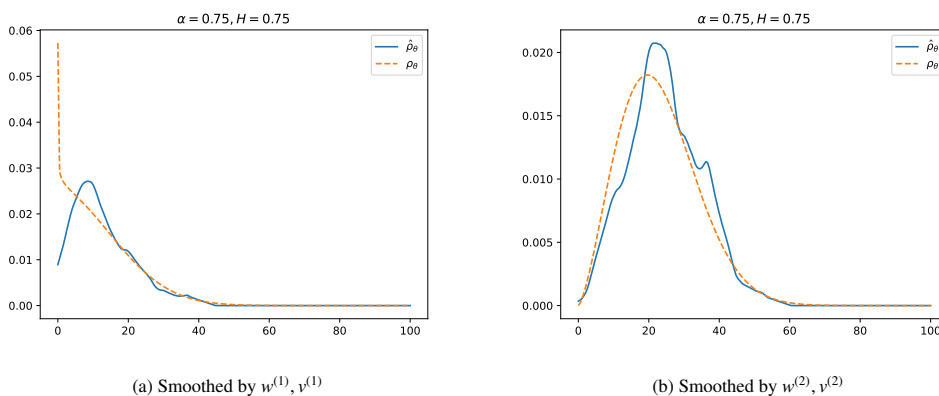


Figure 4: Spectral density estimation for the mollified process for the cases $(\alpha, H) = (0.75, 0.75)$. Estimation is based on a single path realization of X^H equidistantly sampled with $\delta = 0.01$ and $n = 10000$.

5.3. Gamma distribution based estimation of α and H

We now consider the case when it is explicitly known that the sample path belongs to a real HFSM. As mentioned before, errors in the estimates $\hat{\rho}_{\theta_i}$, $i = 1, 2$, directly translate to the regression estimator for α . The advantage of estimating the parameters of the Gamma distribution directly, from which we derived estimators for the stability index α and Hurst parameter H in Corollary 2 and 3, lies in avoiding the need of kernel density estimation and the errors that come along with it as mentioned above. On the other hand, for the parameter estimates of the Gamma distribution to work well a large sample size N of estimated frequencies $\{\hat{Z}_{k,n}\}_{k=1}^N$ is needed, which in turn requires the sample size n of path sample points to be large. Therefore, for the next computations we only consider the case $n = 10000$ with $N = 100, 150, 200$.

Table 3 shows the mean bias of the estimators $\tilde{\alpha}$ and \tilde{H} based on Gamma distribution parameter estimation. Again, we consider 1000 simulations of a single path of a real HFSM X^H with $\alpha \in \{0.75, 1.5\}$ and $H \in \{0.25, 0.75\}$, sampled equidistantly with mesh size $\delta = 0.01$ and sample size $n = 10000$. The paths are smoothed with $v^{(i)}$, $i = 1, 2$, of Example 1 and $N = 100, 150, 200$ frequencies of the underlying LePage series are estimated using the periodogram of the mollified sample.

Mean bias $\tilde{\alpha} - \alpha,$ $\tilde{H} - H$	α	δ	0.01					
		N	$\tilde{\alpha}$			\tilde{H}		
			100	150	200	100	150	200
$w_{20}^{(1)}$	0.75	0.25	0.262	0.255	0.251	0.277	0.272	0.263
		0.75	0.290	0.288	0.285	-0.143	-0.137	-0.139
	1.5	0.25	0.070	0.094	0.058	0.150	0.102	0.051
		0.75	0.066	0.086	0.054	0.012	0.020	-0.006
$w_{20}^{(2)}$	0.75	0.25	0.255	0.244	0.236	0.252	0.261	0.257
		0.75	0.281	0.283	0.259	-0.172	-0.147	-0.171
	1.5	0.25	0.081	0.104	0.061	0.198	0.152	0.096
		0.75	0.093	0.099	0.067	-0.072	-0.051	-0.056

Table 3: Mean bias of the estimators $\hat{\alpha}$ to α based on on the log-transformed ratio $\hat{\rho}_{\theta_1}/\hat{\rho}_{\theta_2}$ with $\theta_1 = 20$, $\theta_2 = 30$. Computations are based on 1000 single path simulations and spectral density estimation for each path, respectively. Each path is sampled equidistantly with mesh size $\delta = 0.01$ and sample size $n = 1000$ and $n = 10000$, respectively.

The estimators perform well in the case $\alpha = 1.5$ for all $H \in \{0.25, 0.75\}$. As expected, the bias of $\tilde{\alpha}$ and \tilde{H} decreases with increasing number of frequencies N fed to the estimators. For small α , i.e. $\alpha = 0.75$ in our case, we see that both estimators for α and H have difficulty assessing their true counterparts. This is mainly due to the same issue we encounter in spectral density estimation for small α , meaning that a handful amplitudes are dominating over the rest since the sequence $\{\Gamma_k^{-1/\alpha}\}_{k=1}^\infty$ decays faster for smaller α .

Remark 6. By [43, Theorem 3.2] and the delta method it holds that the estimators \tilde{b}, \tilde{r} are asymptotically normal with asymptotic covariance matrix

$$\Sigma = \begin{pmatrix} \sigma_b^2 & \sigma_{br} \\ \sigma_{br} & \sigma_r^2 \end{pmatrix},$$

where

$$\sigma_b^2 = b^2(1 + b\Psi_1(1 + b)), \quad \sigma_r^2 = r^2(1 + b\Psi_1(b)), \quad \sigma_{br} = -br(1 + b\Psi_1(1 + b)),$$

and $\Psi_1(x) = d^2/dx^2 \log(\Gamma(x))$ is the trigamma function. Aiming to minimize the Frobenius norm of Σ , given by

$$\|\Sigma\| = \sqrt{b^4(1 + b\Psi_1(1 + b))^2 + r^4(1 + b\Psi_1(b))^2 + 2b^2r^2(1 + b\Psi_1(1 + b))^2},$$

we first see that it is monotonically increasing in b, r . From Corollary 2 we know that

$$b = \frac{\alpha}{q}(p - H), \quad r = \frac{\alpha}{\theta q}, \quad p, q \geq 1,$$

which suggests that, in theory, $p \geq 1$ should be chosen as small as possible, i.e. $p = 1$, and $q \geq 1$ as large as possible, leading to no immediate practical choice of p, q .

In practice however, due to problems in estimating frequencies close to 0, the condition $\alpha(p - H) - 1 > 0$ is favorable so that the spectral density ρ_θ of the mollified process \tilde{X}_θ in Corollary 2 vanishes at the origin, cf. Figure 4. This indicates the lower bound $p \geq \max\{1, 1/\alpha + H\}$. A more conservative bound is given by $p \geq 1/\alpha + 1$, since $H \in (0, 1)$. On the other hand, choosing p too conservatively, i.e. too large, results in fluctuations of $v = \mathcal{F}^{-1}w$ at its tails, see Figure 5 (a).

Furthermore, concerning the choice of the parameter $q \geq 1$, note that $q = 2$ allows for the explicit computation of the smoothing kernel $v = \mathcal{F}^{-1}w$, see Example 1. In general, the function v cannot be given for $q > 2$. Exceptions are the cases with even integers $q > 2$, for which v can be expressed as a sum of generalized hypergeometric functions. Numerical computations show that for $w(x) = x^2 e^{-x^q}$, $q > 2$, the function $v = \mathcal{F}^{-1}w$ exhibits stronger fluctuations at its tails and slower absolute decay compared to the case $q = 2$, compare Figure 5 (b).

Recall that v_θ needs to be discretized at the points $\{\delta(-L/2 + j)\}_{j=0}^L$ for the discrete convolution in the computation of \tilde{X}_θ . The mesh size δ and the number of convolution point L (which depends on the sample size n by $n - L > n_0$ with minimal sample size n_0 for the mollified process) dictate the choice of the parameters θ, p and q such that $|v_\theta(t)| < \varepsilon$ for $t \notin [-\delta L/2, \delta L/2] = I$ and some small error $\varepsilon > 0$. Additionally, the quadrature error of the discrete convolution (18) should be minimal.

Let $v \in C^{k+2}([a, b])$ be an arbitrary function, and denote by $I_k(v)$, $k \in \mathbb{N}_0$, the *Newton-Cotes quadrature* for equidistant discretization points, which generalizes common quadrature formulae such as the rectangle ($k = 0$), trapezoid ($k = 1$) or Simpson formula ($k = 2$). The exact integral of v over $[a, b]$ is denoted by $I(v)$. Then, the quadrature error for the discretization of $v_\theta(x) = v(\theta x)$ is given by

$$E_k(v) = |I(v) - I_k(v)| = \begin{cases} C_k v_\theta^{(k+2)}(\xi) = \theta^{k+2} C_k v^{(k+2)}(\xi), & k \text{ even,} \\ C'_k v_\theta^{(k+1)}(\xi) = \theta^{k+1} C'_k v^{(k+1)}(\xi), & k \text{ odd,} \end{cases}$$

where $\xi \in [a, b]$ and C_k, C'_k are constants given in [35, Theorem 9.2].

Slower decay and fluctuations at the tail of v_θ for larger p and q require a larger choice of θ for v_θ to be negligible outside of the interval I . The above quadrature error indicates that larger values of θ increase the quadrature error, which directly translates to the discrete convolution. This is due to the fluctuations of v_θ being compressed onto the interval I by scaling with θ . The inaccuracy of the discretization can only be mitigated by a smaller mesh size δ . Hence, in practice the discrete convolution for the computation of \tilde{X} works best with $p = 2, 4$ and $q = 2$ under the given values of α, δ and L .

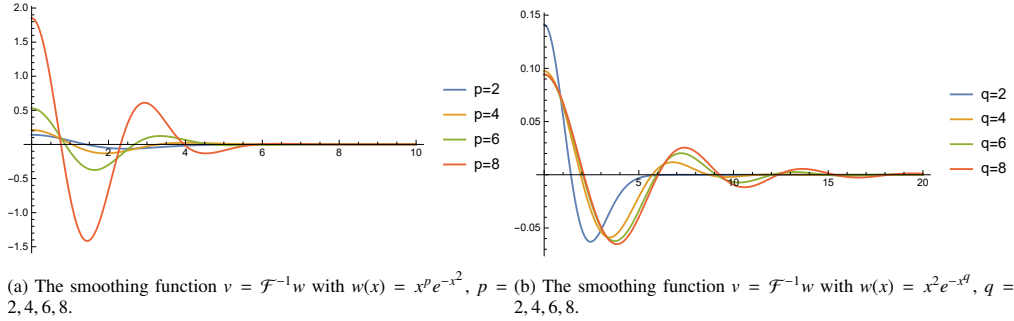


Figure 5: Analysis of $v = \mathcal{F}^{-1}w$ with $w(x) = x^p e^{-x^q}$, $p, q \geq 1$ even.

6. Conclusion

Real harmonizable fractional stable motions are a natural extension of the harmonizable representation of fractional Brownian motions to the stable regime. Opposed to linear fractional stable motions real harmonizable fractional stable motions are non-ergodic deeming standard statistical methods that rely on the law of large numbers for consistency unfeasible.

We consider the more general class of stationary-increment harmonizable stable processes introduced in Equation (5) and give conditions on the integrability of the path of such a process with respect to the measure $\nu(t)dt$ with density $\nu \in L^1(\mathbb{R}) \cap L^2(\mathbb{R})$. Exploiting the integral representation of a stationary-increment harmonizable stable process X and the Fourier transform on the real line, interchanging the order of integration of the convolution $\tilde{X}_\nu(s) = \int_{\mathbb{R}} X(t)\nu(t-s)dt$ allows us to give conditions on $w = \mathcal{F}\nu$ in Theorem 1 such that the mollified process \tilde{X}_ν is a stationary real harmonizable $S\alpha S$ process with integrable spectral density.

Applying periodogram frequency estimation as in [21] yields estimates for the i.i.d. random frequencies of the LePage series representation of the mollified process \tilde{X} . Kernel density estimation allows to assess for the normalized spectral density of \tilde{X}_ν from which we derive methods to estimate the index of stability as well as the integral kernel Ψ of the original stationary-increment harmonizable process X up to a constant factor, see Corollary 1 and Remark 5.

When considering real harmonizable fractional stable motions, the explicit form of Ψ can be taken advantage of. For a specific choice of w and ν given in Corollary 2 the mollified process has underlying random frequencies whose p -th absolute powers (p depending on the choice of the weight function w) are i.i.d. Gamma distributed. The shape and scale parameters of this Gamma distribution can be estimated consistently enabling us to derive consistent estimators for the index of stability α as well as the Hurst parameter H .

In an extensive simulation study we considered 1000 single path realizations of a real harmonizable fractional stable motion. Each path is then smoothed by example functions $\nu^{(1)}$ and $\nu^{(2)}$ with different tuning parameters θ_1, θ_2 , yielding sample paths of a mollified process, which we showed to be a stationary real harmonizable $S\alpha S$ process with finite control measure. We first assume that only the information that all paths are sampled from a stationary-increment harmonizable stable process is given. We estimate the stability index α based on a regression of the log-transformed ratio of two spectral densities from the same path and the same smoothing function $\nu^{(i)}$ but different tuning parameters θ_1, θ_2 as described in Section 4.2. From the estimates of the spectral density and index of stability it is then possible to reconstruct the kernel in the integral representation of a stationary increment harmonizable process up to a constant factor.

Lastly, provided that the process is a real harmonizable fractional stable motion, we can estimate α and the Hurst parameter H as described in Section 4.3. This approach eliminates problems that might arise from inaccurate kernel density estimation, but requires a large number of estimated frequencies N from the periodogram, which in turn dictates larger sample sizes n .

In our experiments, all estimation procedures work well for larger α , i.e. for $\alpha = 1.5$. When the index of stability α is small, estimating the underlying random frequencies via the locations of the peaks in the periodogram is difficult. In this case a small number of amplitudes R_k , recall Equation (10), dominate the rest since the decay of $\Gamma_k^{-1/\alpha}$ as $k \rightarrow \infty$ is faster for small values of α . The periodogram will exhibit strong sidelobe oscillations at the frequencies corresponding to these few dominating amplitudes. The sidelobes might not be completely filtered out during the iterative computation of the frequencies which can hinder the precise estimation of the true underlying frequencies $|Z_{[k]}|$. Smoothing the periodogram or considering different window functions can reduce sidelobe effects but at the cost of precision for the frequency estimation. Other sources of error lie in the discretization in the simulation of the samples as well as the discrete convolution.

Summarizing, our proposed methods achieve accurate results as long as the underlying frequency estimation is accurate. All methods are computationally efficient since discrete convolution and periodogram computation with the fast Fourier transform are computationally inexpensive. Most notably, frequency estimation via the periodogram circumvents the problem of non-ergodicity. Results can be improved if the frequency estimation becomes more accurate.

References

- [1] A. Ayache. Harmonizable fractional stable motion: simultaneous estimators for the both parameters. *Preprint*, HAL Id: hal-04091407, 2023.
- [2] A. Ayache and G. Boutard. Stationary increments harmonizable stable fields: upper estimates on path behaviour. *J. Theoret. Probab.*, 30(4):1369–1423, 2017.
- [3] A. Ayache and J. Hamonier. Linear fractional stable motion: a wavelet estimator of the α parameter. *Statist. Probab. Lett.*, 82(8):1569–1575, 2012.
- [4] A. Ayache and J. Hamonier. Linear multifractional stable motion: fine path properties. *Rev. Mat. Iberoam.*, 30(4):1301–1354, 2014.
- [5] A. Ayache and Y. Xiao. Harmonizable fractional stable fields: local nondeterminism and joint continuity of the local times. *Stochastic Process. Appl.*, 126(1):171–185, 2016.
- [6] A. Ayache, N.-R. Shieh, and Y. Xiao. Wavelet series representation and geometric properties of harmonizable fractional stable sheets. *Stochastics*, 92(1):1–23, 2020.
- [7] A. Basse-O’Connor and M. Podolskij. Asymptotic theory for quadratic variation of harmonizable fractional stable processes. *Theory Probab. Math. Statist.*, (110):3–12, 2024.
- [8] A. Basse-O’Connor, R. Lachièze-Rey, and M. Podolskij. Power variation for a class of stationary increments Lévy driven moving averages. *Ann. Probab.*, 45(6B):4477–4528, 2017.
- [9] J. Beran. *Statistics for long-memory processes*. Routledge, 2017.
- [10] H. Biermé, M. Meerschaert, and H.-P. Scheffler. Operator scaling stable random fields. *Stochastic Process. Appl.*, 117(3):312–332, 2007.
- [11] S. Cambanis and M. Maejima. Two classes of self-similar stable processes with stationary increments. *Stochastic Process. Appl.*, 32(2):305–329, 1989.
- [12] S. Cambanis and A. R. Soltani. Prediction of stable processes: Spectral and moving average representation. *Z. Wahrscheinlichkeitstheorie verw. Gebiete*, 66(4):563–612, 1984.
- [13] S. Cambanis, C. D. Hardin, Jr., and A. Weron. Ergodic properties of stationary stable processes. *Stochastic Process. Appl.*, 24(1):1–18, 1987.
- [14] R. Dahlhaus. Efficient parameter estimation for self-similar processes. *Ann. Statist.*, 17(4):1749–1766, 1989.
- [15] H. Drygas. Weak and strong consistency of the least squares estimators in regression models. *Z. Wahrscheinlichkeitstheorie und Verw. Gebiete*, 34(2):119–127, 1976.
- [16] P. Embrechts and M. Maejima. *Self-similar processes*. Princeton Series in Applied Mathematics. Princeton University Press, Princeton, NJ, 2002.

- [17] R. Fox and M. S. Taqqu. Large-sample properties of parameter estimates for strongly dependent stationary Gaussian time series. *Ann. Statist.*, 14(2):517–532, 1986.
- [18] L. Grafakos. *Classical fourier analysis*, volume 2. Springer, New York, 2008.
- [19] E. J. Hannan. The estimation of frequency. *J. Appl. Probab.*, 10(3):510–519, 1973.
- [20] L. V. Hoang and E. Spodarev. Inversion of α -sine and α -cosine transforms on \mathbb{R} . *Inverse Problems*, 37(8), 2021.
- [21] L. V. Hoang and E. Spodarev. Non-ergodic statistics and spectral density estimation for stationary real harmonizable symmetric α -stable processes. *Bernoulli*, To appear, 2024.
- [22] O. Kallenberg. *Foundations of Modern Probability*. Springer, 2002.
- [23] I. Karatzas and S. Shreve. *Brownian Motion and Stochastic Calculus*. Graduate Texts in Mathematics. Springer New York, 2014.
- [24] A. N. Kolmogoroff. Wienersche Spiralen und einige andere interessante Kurven im Hilbertschen Raum. *C. R. (Doklady) Acad. Sci. URSS (N.S.)*, 26:115–118, 1940.
- [25] N. Kôno and M. Maejima. Self-similar stable processes with stationary increments. In *Stable processes and related topics (Ithaca, NY, 1990)*, volume 25 of *Progr. Probab.*, pages 275–295. Birkhäuser Boston, Boston, MA, 1991.
- [26] J. Lamperti. Semi-stable stochastic processes. *Trans. Am. Math. Soc.*, 104(1):62–78, 1962.
- [27] M. M. Ljungdahl and M. Podolskij. A minimal contrast estimator for the linear fractional stable motion. *Stat. Inference Stoch. Process.*, 23(2):381–413, 2020.
- [28] B. B. Mandelbrot and M. S. Taqqu. Robust R/S analysis of long-run serial correlation. *Bull. Inst. Internat. Statist.*, 48(2):69–99, 1979.
- [29] B. B. Mandelbrot and J. W. Van Ness. Fractional Brownian motions, fractional noises and applications. *SIAM Rev.*, 10(4):422–437, 1968.
- [30] B. B. Mandelbrot and J. R. Wallis. Computer experiments with fractional Gaussian noises: Part 1, averages and variances. *Water Resour. Res.*, 5(1):228–241, 1969.
- [31] B. B. Mandelbrot and J. R. Wallis. Computer experiments with fractional Gaussian noises: Part 2, rescaled ranges and spectra. *Water Resour. Res.*, 5(1):242–259, 1969.
- [32] B. B. Mandelbrot and J. R. Wallis. Computer experiments with fractional gaussian noises: Part 3, mathematical appendix. *Water Resour. Res.*, 5(1):260–267, 1969.
- [33] S. Mazur, D. Otryakhin, and M. Podolskij. Estimation of the linear fractional stable motion. *Bernoulli*, 26(1): 226–252, 2020.
- [34] T. Mikosch, S. Resnick, H. Rootzén, and A. Stegeman. Is network traffic approximated by stable Lévy motion or fractional Brownian motion? *Ann. Appl. Probab.*, 12(1):23–68, 2002.
- [35] A. Quarteroni, R. Sacco, and F. Saleri. *Numerical mathematics*. Springer-Verlag, Berlin, 2007.
- [36] B. G. Quinn and E. J. Hannan. *The Estimation and Tracking of Frequency*. Cambridge University Press, 2001.
- [37] J. Rosinski. On the structure of stationary stable processes. *Ann. Probab.*, 23(3):1163–1187, 1995.
- [38] G. Samorodnitsky. Integrability of stable processes. *Probab. Math. Statist.*, 13(2):191–204, 1992.
- [39] G. Samorodnitsky and M. S. Taqqu. The various linear fractional Lévy motions. In *Probability, statistics, and mathematics*, pages 261–270. Academic Press, Boston, MA, 1989.
- [40] G. Samorodnitsky and M. S. Taqqu. *Stable Non-Gaussian Random Processes: Stochastic Models with Infinite Variance*. Chapman and Hall, 1994.
- [41] S. Stoev, V. Pipiras, and M. S. Taqqu. Estimation of the self-similarity parameter in linear fractional stable motion. *Signal Processing*, 82(12):1873–1901, 2002.
- [42] W. Willinger, V. Paxson, and M. S. Taqqu. Self-similarity and heavy tails: Structural modeling of network traffic. *A practical guide to heavy tails: statistical techniques and applications*, 23(1):27–53, 1998.
- [43] Z.-S. Ye and N. Chen. Closed-form estimators for the Gamma distribution derived from likelihood equations. *The American Statistician*, 71(2):177–181, 2017.

Appendix A. On the non-ergodicity of stationary real harmonizable stable processes

For the fundamentals on ergodic theory for stationary processes, in particular, basics such as measure-preserving transforms, invariant sets and Birkhoff's ergodic theorem, we refer to [22, Chapter 10]. The σ -algebra of invariant sets of a stationary real harmonizable $S\alpha S$ process X is given by $\sigma(\{\Gamma_k^{-1/\alpha} G_k^{(1)}, \Gamma_k^{-1/\alpha} G_k^{(2)}, Z_k\}_{k \in \mathbb{N}})$, where the sequences of random variables $\{\Gamma_k\}_{k \in \mathbb{N}}$, $\{G_k^{(j)}\}_{k \in \mathbb{N}}$, $j = 1, 2$, and $\{Z_k\}_{k \in \mathbb{N}}$ are the same as in the LePage series representation (9) [21, Theorem 3].

From its series representation (9) it becomes immediately apparent that the process X is stationary Gaussian conditional on the sequences $\{\Gamma_k\}_{k \in \mathbb{N}}$ and $\{Z_k\}_{k \in \mathbb{N}}$. In fact, conditional on $\{\Gamma_k\}_{k \in \mathbb{N}}$ and $\{Z_k\}_{k \in \mathbb{N}}$, it is a so-called Gaussian harmonic process, which is a series of sinusoidal waves with (conditional) Gaussian amplitudes and frequencies $\{Z_k\}_{k \in \mathbb{N}}$ with (conditional) covariance function

$$\mathbb{E}[X(s)X(t) \mid \{\Gamma_k\}_{k \in \mathbb{N}}, \{Z_k\}_{k \in \mathbb{N}}] = C_\alpha^2 m(\mathbb{R})^{2/\alpha} \sum_{k=1}^{\infty} \Gamma_k^{-2/\alpha} \cos((t-s)Z_k),$$

compare [40, Proposition 6.6.4]. The spectral measure (from the Gaussian spectral theory, not to be mistaken for the spectral measure of a stable random vector) corresponding to the above covariance function is purely atomic and concentrated at the absolute frequencies $\{|Z_k|\}_{k \in \mathbb{N}}$.

Appendix B. Proof of Theorem 1

The proof of Theorem 1 requires the introduction of the so-called α -sine transform given by

$$\mathcal{T}_\alpha u(t) = \int_{\mathbb{R}} |\sin(tx)|^\alpha u(x) dx$$

for $\alpha \in (0, 2)$, which is well-defined for $u \in L^1(\mathbb{R}, \min(1, |x|^\alpha) dx)$. It is easy to see that if u is an even function, then $\mathcal{T}_\alpha u$ is even as well and $\mathcal{T}_\alpha u(0) = 0$.

The following lemma describes the behavior of $\mathcal{T}_\alpha u$ at the origin and its tails, which will be useful for the proof of Theorem 1. We say that two functions $f(x)$ and $g(x)$ are asymptotically equivalent as $x \rightarrow x_0$ if $\lim_{x \rightarrow x_0} f(x)/g(x) = 1$ and write $f(x) \sim g(x)$ as $x \rightarrow x_0$.

Lemma 2. *Let $\alpha \in (0, 2)$ and $u \in L^1(\mathbb{R}, \min(1, |x|^\alpha) dx)$ be even. Then,*

- (i) $\mathcal{T}_\alpha u(t) \sim |t|^\alpha$ as $t \rightarrow 0$.
- (ii) $\mathcal{T}_\alpha |u|(t) \sim |t|^{\alpha+\beta-1}$ as $|t| \rightarrow \infty$ for some $\beta < 1$.
- (iii) If $u \in L^1(\mathbb{R})$, then $\mathcal{T}_\alpha u$ is bounded by $\|u\|_1$. Furthermore, $\mathcal{T}_\alpha u(t) \rightarrow c_0(\alpha)\|u\|_1$ as $|t| \rightarrow \infty$, where the constant $c_0(\alpha)$ is given by $c_0(\alpha) = 2^{-\alpha}\Gamma(1+\alpha)/\Gamma(1+\alpha/2)^2$.

Proof. (i) Follows directly from the definition of \mathcal{T}_α as $\sin(t) \sim |t|$ as $t \rightarrow 0$.

- (ii) Since $\mathcal{T}_\alpha u$ is even, consider just $t > 0$. The substitution $y = tx$ in the definition of $\mathcal{T}_\alpha |u|$ yields

$$\mathcal{T}_\alpha |u|(t) = \int_{\mathbb{R}} |\sin(y)|^\alpha \left| u\left(\frac{y}{t}\right) \right| t^{-1} dy.$$

The behavior of $\mathcal{T}_\alpha|u|(t)$ as $t \rightarrow \infty$ is therefore determined by the behavior of $|u(x)|$ as $x \rightarrow 0$. Since $u \in L^1(\mathbb{R}, \min(1, |x|^\alpha)dx)$ needs to hold for $\mathcal{T}_\alpha u$ to be well-defined, it follows that $|u(x)|x^\alpha \sim x^{-\beta}$ as $x \rightarrow 0$ for some $\beta < 1$, thus $|u(x)| \sim x^{-\alpha-\beta}$ as $x \rightarrow 0$. It follows that

$$\left|u\left(\frac{y}{t}\right)\right|t^{-1} \sim \left(\frac{y}{t}\right)^{-\alpha-\beta}t^{-1} = yt^{\alpha+\beta-1}$$

as $t \rightarrow \infty$ and consequently as $\mathcal{T}_\alpha|u|(t) \sim t^{\alpha+\beta-1}$ as $t \rightarrow \infty$ for some $\beta < 1$.

(iii) By the triangle inequality we have

$$|\mathcal{T}_\alpha u(t)| \leq \int_{\mathbb{R}} |\sin(tx)|^\alpha |u(x)| dx \leq \int_{\mathbb{R}} |u(x)| dx = \|u\|_1.$$

Furthermore, for $u \in L^1(\mathbb{R})$ the α -sine transform admits the series representation

$$\mathcal{T}_\alpha u(t) = c_0 \mathcal{F}u(0) + 2 \sum_{k=1}^{\infty} c_k \mathcal{F}u(2kt),$$

with coefficients

$$c_k = c_k(\alpha) = \frac{(-1)^k}{2^\alpha} \frac{\Gamma(1+\alpha)}{\Gamma(1+\alpha/2-k)\Gamma(1+\alpha/2+k)},$$

see [20, Theorem 2]. Additionally, the series $\sum_{k=1}^{\infty} c_k$ converges absolutely to $c_0/2$ [20, Corollary 2]. The Fourier transform $\mathcal{F}u$ is bounded by $\|u\|_1$ and vanishes at its tails. Also, $\mathcal{F}u(0) = \|u\|_1$ holds. Hence, the dominated convergence theorem yields $\mathcal{T}_\alpha u(t) \rightarrow c_0 \|u\|_1$ as $t \rightarrow \infty$ and c_0 can be computed from the above expression for the coefficients c_k , i.e.

$$c_0 = 2^{-\alpha} \frac{\Gamma(1+\alpha)}{\Gamma\left(1+\frac{\alpha}{2}\right)^2}.$$

□

We now turn to the proof of Theorem 1.

Proof of Theorem 1. In general, necessary and sufficient conditions for the p -integrability of α -stable processes with integral representation $X(t) = \int_E h_t(x) M_\alpha(dx)$ are given in [38, Theorem 3.3], see also [40, Chapter 11.3]. Setting $p = 1$ and $h_t(x) = (e^{itx} - 1)\Psi(x)$ yields that

$$\int_{\mathbb{R}} |X(t)|v(t)dt < \infty \quad a.s.$$

if and only if one of the following conditions is met (depending on α):

(i) Case $\alpha \in (0, 1)$:

$$\int_{\mathbb{R}} \left(\int_{\mathbb{R}} |(e^{itx} - 1)\Psi(x)|v(t)dt \right)^\alpha dx < \infty. \quad (\text{B.1})$$

(ii) Case $\alpha \in (1, 2)$:

$$\int_{\mathbb{R}} \left(\int_{\mathbb{R}} |(e^{itx} - 1) \Psi(x)|^\alpha dx \right)^{1/\alpha} v(t) dt < \infty. \quad (\text{B.2})$$

(iii) Case $\alpha = 1$:

$$\begin{aligned} & \int_{\mathbb{R}} \left(\int_{\mathbb{R}} |(e^{itx} - 1) \Psi(x)| \right. \\ & \times \left. \left[1 + \log_+ \left(\frac{\left| (e^{itx} - 1) \Psi(x) \right| \int_{\mathbb{R}} \int_{\mathbb{R}} |(e^{isy} - 1) \Psi(y)| v(s) ds dy}{\left(\int_{\mathbb{R}} |(e^{ity} - 1) \Psi(y)| dy \right) \left(\int_{\mathbb{R}} |(e^{isx} - 1) \Psi(x)| v(s) ds \right)} \right) \right] dx \right) v(t) dt < \infty, \end{aligned} \quad (\text{B.3})$$

where $\log_+(x) = \max\{0, \log(x)\}$.

Rewriting $|(e^{itx} - 1) \Psi(x)| = 2 |\sin(tx/2)| |\Psi(x)|$ for all $t, x \in \mathbb{R}$ we get:

(i) Case $\alpha \in (0, 1)$:

$$\begin{aligned} \int_{\mathbb{R}} \left(\int_{\mathbb{R}} |(e^{itx} - 1) \Psi(x)| v(t) dt \right)^\alpha dx &= 2^\alpha \int_{\mathbb{R}} \left(\int_{\mathbb{R}} \left| \sin\left(\frac{tx}{2}\right) \right| v(t) dt \right)^\alpha |\Psi(x)|^\alpha dx \\ &= 2^\alpha \int_{\mathbb{R}} \left(\mathcal{T}_1 v\left(\frac{x}{2}\right) \right)^\alpha |\Psi(x)|^\alpha dx < \infty, \end{aligned}$$

since $\mathcal{T}_1 v(x) \sim |x|$ as $x \rightarrow 0$, which implies $(\mathcal{T}_1 v(x))^\alpha \sim |x|^\alpha$ as $x \rightarrow 0$, and $\mathcal{T}_1 v(x) \rightarrow c_0(1) \|v\|_1$ as $|x| \rightarrow \infty$ for $v \in L^1(\mathbb{R})$ by Lemma 2(i) and (iii). The finiteness of the above integral then follows from the fact that Ψ lies in the space $L^\alpha(\mathbb{R}, \min(1, |x|^\alpha) dx)$.

(ii) Case $\alpha \in (1, 2)$:

$$\begin{aligned} \int_{\mathbb{R}} \left(\int_{\mathbb{R}} |(e^{itx} - 1) \Psi(x)|^\alpha dx \right)^{1/\alpha} v(t) dt &= 2 \int_{\mathbb{R}} \left(\int_{\mathbb{R}} \left| \sin\left(\frac{tx}{2}\right) \right|^\alpha |\Psi(x)|^\alpha dx \right)^{1/\alpha} v(t) dt \\ &= 2 \int_{\mathbb{R}} \left(\mathcal{T}_\alpha |\Psi|\left(\frac{t}{2}\right) \right)^{1/\alpha} v(t) dt < \infty. \end{aligned}$$

By Lemma 2(ii) it holds that $\mathcal{T}_\alpha |\Psi|(t) \sim |t|^{\alpha+\beta-1}$, $\beta < 1$, as $|t| \rightarrow \infty$, hence

$$(\mathcal{T}_\alpha |\Psi|(t))^{1/\alpha} \sim |t|^{1+(\beta-1)/\alpha}.$$

Note that $1 + (\beta - 1)/\alpha < 1$ as $\beta < 1$, thus

$$\int_{\mathbb{R}} \left(\mathcal{T}_\alpha |\Psi|\left(\frac{t}{2}\right) \right)^{1/\alpha} v(t) dt < \infty$$

if $v \in L^1(\mathbb{R}, \max(1, |t|) dt)$. This is guaranteed since $v = \mathcal{F}^{-1} w$ is continuous, $v(0) = \|w\|_1 / (2\pi)$ and $v(t) = \mathcal{F}^{-1} w(t) = o(|t|^{-3})$ as $|t| \rightarrow \infty$ due to $w \in W^{1,3}(\mathbb{R})$.

(iii) Case $\alpha = 1$: Note that monotonicity of the logarithm and the triangle inequality allows us to bound the absolute value of the double integral in Equation (B.3) from above by replacing v with $|v|$. Without loss of generality v can therefore be assumed to be non-negative. Also,

note that $1 + \log_+(z) \leq 1 + z$ for all $z \geq 0$, which allows us to bound Equation (B.3) from above by

$$\int_{\mathbb{R}} \left(\int_{\mathbb{R}} |h_t(x)| dx \right) v(t) dt + \int_{\mathbb{R}} \left(\int_{\mathbb{R}} |h_t(x)| \frac{|h_t(x)| \int_{\mathbb{R}} \left(\int_{\mathbb{R}} |h_s(y)| v(s) ds \right) dy}{\left(\int_{\mathbb{R}} |h_t(y)| dy \right) \left(\int_{\mathbb{R}} |h_s(x)| v(s) ds \right)} dy \right) v(t) dt = I_1 + I_2.$$

The first double integral is given by

$$I_1 = 2 \int_{\mathbb{R}} \left(\int_{\mathbb{R}} \left| \sin \left(\frac{tx}{2} \right) \right| |\Psi(x)| dx \right) v(t) dt = 2 \int_{\mathbb{R}} \mathcal{T}_1 |\Psi| \left(\frac{t}{2} \right) v(t) dt < \infty,$$

by the same argument as in the case $\alpha \in (1, 2)$.

We can simplify the expression inside the second double integral I_2 by

$$\begin{aligned} & |h_t(x)| \frac{|h_t(x)| \int_{\mathbb{R}} \left(\int_{\mathbb{R}} |h_s(y)| v(s) ds \right) dy}{\left(\int_{\mathbb{R}} |h_t(y)| dy \right) \left(\int_{\mathbb{R}} |h_s(x)| v(s) ds \right)} \\ &= 4 \left| \sin \left(\frac{tx}{2} \right) \right|^2 |\Psi(x)|^2 \frac{2 \int_{\mathbb{R}} \left(\int_{\mathbb{R}} \left| \sin \left(\frac{sy}{2} \right) \right| |\Psi(y)| v(s) ds \right) dy}{2 \left(\int_{\mathbb{R}} \left| \sin \left(\frac{ty}{2} \right) \right| |\Psi(y)| dy \right) \left(2 |\Psi(x)| \int_{\mathbb{R}} \left| \sin \left(\frac{sx}{2} \right) \right| v(s) ds \right)} \\ &= \left| \sin \left(\frac{tx}{2} \right) \right|^2 |\Psi(x)| \frac{2 \int_{\mathbb{R}} \mathcal{T}_1 |\Psi| \left(\frac{s}{2} \right) v(s) ds}{\mathcal{T}_1 |\Psi| \left(\frac{t}{2} \right) \mathcal{T}_1 v \left(\frac{x}{2} \right)} = \left| \sin \left(\frac{tx}{2} \right) \right|^2 |\Psi(x)| \frac{I_1}{\mathcal{T}_1 |\Psi| \left(\frac{t}{2} \right) \mathcal{T}_1 v \left(\frac{x}{2} \right)}, \end{aligned}$$

which yields

$$\begin{aligned} I_2 &= I_1 \int_{\mathbb{R}} \left(\int_{\mathbb{R}} \left| \sin \left(\frac{tx}{2} \right) \right|^2 |\Psi(x)| \frac{1}{\mathcal{T}_1 |\Psi| \left(\frac{t}{2} \right) \mathcal{T}_1 v \left(\frac{x}{2} \right)} dx \right) v(t) dt \\ &= I_1 \int_{\mathbb{R}} \underbrace{\left(\int_{\mathbb{R}} \left| \sin \left(\frac{tx}{2} \right) \right|^2 |\Psi(x)| \left(\mathcal{T}_1 v \left(\frac{x}{2} \right) \right)^{-1} dx \right)}_{=: J(t)} \left(\mathcal{T}_1 |\Psi| \left(\frac{t}{2} \right) \right)^{-1} v(t) dt. \end{aligned}$$

Note that $|\sin(tx/2)|^2 (\mathcal{T}_1 v(x/2))^{-1}$ is bounded for all $t, x \in \mathbb{R}$ and behaves asymptotically like $t^2|x|/4$ as $x \rightarrow 0$ for all $t \in \mathbb{R}$. Since $\Psi \in L^1(\mathbb{R}, \min(1, |x|) dx)$, the function J is well defined on \mathbb{R} . Moreover, it holds that $J(t) = O(t^2)$ as $t \rightarrow 0$ and for $t \rightarrow \infty$ the substitution $y = tx/2$ yields

$$J(t) = 2 \int_{\mathbb{R}} |\sin(y)|^2 \underbrace{\left(\mathcal{T}_1 v \left(\frac{y}{t} \right) \right)^{-1}}_{=O(1/|t|^{-1})=O(|t|)} \underbrace{\left| \Psi \left(\frac{2y}{t} \right) \right| \frac{1}{|t|}}_{=O(|t|^{1+\beta-1})=O(|t|^\beta)} dy = O(|t|^{1+\beta}).$$

Consequently, we have

$$J(t) \left(\mathcal{T}_1 |\Psi| \left(\frac{t}{2} \right) \right)^{-1} = \begin{cases} O(t^2/|t|) = O(|t|), & t \rightarrow 0, \\ O(|t|^{1+\beta}/|t|^\beta) = O(|t|), & |t| \rightarrow \infty \end{cases}$$

and

$$\int_{\mathbb{R}} J(t) \left(\mathcal{T}_1 |\Psi| \left(\frac{t}{2} \right) \right)^{-1} v(t) dt < \infty$$

for $v \in L^1(\mathbb{R}, \max(1, |t|) dt)$, which is again fulfilled due to $w \in W^{1,3}(\mathbb{R})$ as in the case $\alpha \in (1, 2)$.

Ultimately, the almost sure integrability in Equation (7) follows under the given assumptions and is still guaranteed under scaling and translation of the function v . Furthermore, it is easy to see that for the mollified process $\tilde{X}_v(s) = \int_{\mathbb{R}} X(t) v(t-s) dt$ we have

$$\tilde{X}_v(s) = \int_{\mathbb{R}} \operatorname{Re} \left(\int_{\mathbb{R}} h_t(x) M_\alpha(dx) \right) v(t-s) dt = \operatorname{Re} \left(\int_{\mathbb{R}} \left(\int_{\mathbb{R}} h_t(x) M_\alpha(dx) \right) v(t-s) dt \right)$$

since v is real valued. Hence, applying [38, Theorem 4.1] yields

$$\begin{aligned} \tilde{X}(s) &\stackrel{a.s.}{=} \operatorname{Re} \left(\int_{\mathbb{R}} \left(\int_{\mathbb{R}} (e^{itx} - 1) \Psi(x) v(t-s) dt \right) M_\alpha(dx) \right) \\ &= \operatorname{Re} \left(\int_{\mathbb{R}} \left(\underbrace{\int_{\mathbb{R}} e^{itx} v(t-s) dt}_{=e^{isx} \int_{\mathbb{R}} e^{itx} v(t) dt} - \underbrace{\int_{\mathbb{R}} v(t-s) dt}_{=w(0)=0} \right) \Psi(x) M_\alpha(dx) \right) \\ &= \operatorname{Re} \left(\int_{\mathbb{R}} e^{isx} w(x) \Psi(x) M_\alpha(dx) \right). \end{aligned}$$

The random measure $\tilde{M}_\alpha(dx) = w(x) \Psi(x) M_\alpha(dx)$ is complex isotropic $S\alpha S$ with control measure $\tilde{m}(dx) = |w(x) \Psi(x)|^\alpha dx$. The new control measure \tilde{m} is finite since the function $w\Psi$ lies in the space $L^\alpha(\mathbb{R})$, which concludes this proof. \square

Appendix C. Additional tables

Median squared L^2 -dist. $\ \hat{\rho} - \rho\ _2^2 (\times 10^{-3})$	α	δ	0.01					
		n	10^3			10^4		
		N	10	25	40	100	150	200
		H						
$w_{20}^{(1)}$	0.75	0.25	4.376	1.155	0.594	3.512	2.873	2.166
		0.75	5.156	1.719	2.132	4.022	3.198	2.468
	1.5	0.25	1.236	0.510	1.126	0.446	0.278	0.214
		0.75	1.235	0.509	1.287	0.459	0.279	0.232
$w_{20}^{(2)}$	0.75	0.25	3.863	1.443	0.730	3.284	2.916	2.349
		0.75	4.301	1.400	0.674	3.317	2.829	2.341
	1.5	0.25	1.270	0.452	1.038	0.465	0.284	0.213
		0.75	1.239	0.444	1.037	0.453	0.275	0.206

Table C.4: Median squared L^2 -distances between kernel density estimators $\hat{\rho}_\theta$ and normalized spectral density ρ_θ over the interval $[0, 100]$. Same setting as in Table 2.

Number of estimates $\hat{\alpha} \notin (0, 2)$	α	δ	0.01					
		n	10^3			10^4		
		N	10	25	40	100	150	200
		H						
$w_{20}^{(1)}$	0.75	0.25	320	110	31	152	128	75
		0.75	344	119	53	204	143	91
	1.5	0.25	364	28	4	159	79	29
		0.75	442	68	4	242	132	38
$w_{20}^{(2)}$	0.75	0.25	334	114	43	202	162	112
		0.75	329	112	35	179	140	90
	1.5	0.25	396	154	2	235	186	128
		0.75	378	82	1	202	126	75

Table C.5: Supplementary table to Table 1. Number of estimates $\hat{\alpha} \notin (0, 2)$.